Biomedicine & Pharmacotherapy 176 (2024) 116907

Contents lists available at ScienceDirect

Biomedicine & Pharmacotherapy

journal homepage: www.elsevier.com/locate/biopha

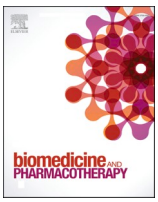

(Homo-)harringtonine prevents endothelial inflammation through IRF-1 dependent downregulation of VCAM1 mRNA expression and inhibition of cell adhesion molecule protein biosynthesis

Luisa D. Burgers [a,1], Sarah Ciurus [a,1], Patrick Engel [c], Silvia Kuntschar [d], Rebecca Raue [d], Anastasiia Kiprina [d], Tobias Primke [a], Tobias Schmid [d], Andreas Weigert [d], Achim Schmidtko [c], Robert Fürst [a,b,e,*]

[a] Institute of Pharmaceutical Biology, Faculty of Biochemistry, Chemistry and Pharmacy, Goethe University, Frankfurt am Main, Germany
[b] LOEWE Center for Translational Biodiversity Genomics (LOEWE-TBG), Frankfurt am Main, Germany
[c] Institute of Pharmacology and Clinical Pharmacy, Faculty of Biochemistry, Chemistry and Pharmacy, Goethe University, Frankfurt am Main, Germany
[d] Institute of Biochemistry I, Faculty of Medicine, Goethe University, Frankfurt am Main, Germany
[e] Pharmaceutical Biology, Department of Pharmacy – Center for Drug Research, Ludwig-Maximilians-Universität München, Munich, Germany

ARTICLE INFO

Key words:
Inflammation
Cell adhesion
Homoharringtonine
Interferon regulatory factor 1
Mitogen-activated protein kinases
Protein biosynthesis

ABSTRACT

The plant alkaloid homoharringtonine (HHT) is a Food and Drug Administration (FDA)-approved drug for the treatment of hematologic malignancies. In addition to its well-established antitumor activity, accumulating evidence attributes anti-inflammatory effects to HHT, which have mainly been studied in leukocytes to date. However, a potential influence of HHT on inflammatory activation processes in endothelial cells, which are a key feature of inflammation and a prerequisite for the leukocyte-endothelial cell interaction and leukocyte extravasation, remains poorly understood. In this study, the anti-inflammatory potential of HHT and its derivative harringtonine (HT) on the TNF-induced leukocyte-endothelial cell interaction was assessed, and the underlying mechanistic basis of these effects was elucidated. HHT affected inflammation *in vivo* in a murine peritonitis model by reducing leukocyte infiltration and proinflammatory cytokine expression as well as ameliorating abdominal pain behavior. *In vitro*, HT and HHT impaired the leukocyte-endothelial cell interaction by decreasing the expression of the endothelial cell adhesion molecules intracellular adhesion molecule −1 (ICAM-1) and vascular cell adhesion molecule-1 (VCAM-1). This effect was mediated by a bipartite mechanism. While HHT did not affect the prominent TNF-induced pro-inflammatory NF-κB signaling cascade, the compound downregulated the *VCAM1* mRNA expression in an IRF-1-dependent manner and diminished active *ICAM1* mRNA translation as determined by polysome profiling. This study highlights HHT as an anti-inflammatory compound that efficiently hampers the leukocyte-endothelial cell interaction by targeting endothelial activation processes.

1. Introduction

Acute inflammation is the physiological, self-limiting response towards infections, tissue injuries or malfunctions with the purpose of defending the body and restoring homeostasis. During the inflammatory response, cytokines such as the tumor necrosis factor (TNF) are secreted by tissue-resident cells like macrophages and dendritic cells [1]. These cytokines then inflammatorily activate the vascular endothelium, which builds the inner lining of blood vessels [2]. In the following, leukocytes from the blood stream are recruited to the inflamed tissue. This recruitment process is mediated through the interaction of the leukocytes with the activated endothelium, which consists of leukocyte rolling on, firm adhesion to and transmigration through the endothelial monolayer [3].

TNF exerts its pro-inflammatory effects by binding to its cell surface TNF receptor 1 (TNFR1) and, consequently, by initiating downstream

* Corresponding author at: Institute of Pharmaceutical Biology, Faculty of Biochemistry, Chemistry and Pharmacy, Goethe University, Frankfurt am Main, Germany.
E-mail address: robert.fuerst@cup.lmu.de (R. Fürst).
[1] These authors contributed equally to this work and share first authorship

https://doi.org/10.1016/j.biopha.2024.116907
Received 11 March 2024; Received in revised form 5 June 2024; Accepted 6 June 2024
Available online 11 June 2024

nuclear factor kappa B (NF-κB) signaling. Binding of TNF to the TNFR1 leads to the phosphorylation-dependent activation of transforming growth factor-β-activated kinase 1 (TAK1) and IκB kinase α/β (IKKα/β). IKKα/β then phosphorylates members of the inhibitory nuclear factor κB (IκB) family of proteins [4,5]. IκB proteins mask the nuclear localization sequence (NLS) of the NF-κB subunits, including the p65 subunit, thereby retaining them in the cytosol and preventing nuclear translocation. Phosphorylation of IkB proteins promotes their ubiquitination and subsequent proteasomal degradation [6,7]. This process causes exposure of the NLS and, in the following, the interaction of the NF-κB subunits with nuclear import proteins that shuttle the NF-κB subunits to the nucleus [8]. In the nucleus, NF-κB carries out its function as transcription factor through binding to specific binding domains in the promotor region of target genes [9]. These target genes comprise, amongst others, endothelial cell adhesion molecules (CAMs) like E-selectin, intracellular adhesion molecule 1 (ICAM-1) and vascular cell adhesion molecule 1 (VCAM-1). CAMs mediate consecutive steps of the leukocyte adhesion cascade: While E-selectin facilitates the rolling motion of leukocytes on the endothelium, ICAM-1 and VCAM-1 promote the firm adhesion of leukocytes to the endothelial monolayer through interacting with leukocyte cell surface integrins like lymphocyte function-associated antigen 1 (LFA-1) and very late antigen-4 (VLA-4) [10–12].

Besides NF-κB, other transcription factors are involved in the pro-inflammatory gene expression of CAMs as well. Expression of the transcription factor IRF-1 is rapidly induced upon pro-inflammatory activation of cells by cytokines like interferon (IFN) and TNF or by lipopolysaccharides (LPS). IRF-1 has been shown to specifically regulate VCAM-1, but not E-selectin or ICAM-1 expression, independent of NF-κB signaling [13]. GATA-6 transcriptional activity leads to the upregulation of pro-inflammatory mediators, which favors inflammatory processes such as airway inflammation [14]. Repression of GATA-6 protein biosynthesis through inhibition of mechanistic target of rapamycin (mTOR) has been shown to specifically downregulate VCAM-1 expression in aortic endothelial cells [15]. In sum, while both the *ICAM1* and *VCAM1* promotor region contain binding sites for NF-κB and AP-1, IRF-1 and GATA-6 only bind to the promotor of *VCAM1* not *ICAM1* [16–19].

While acute inflammation is a crucial evolutionary process, inflammation can become chronic due to persistence of infections, exaggerated or subnormal immune responses as well as inappropriate resolution. Chronic inflammation leads to severe diseases such as rheumatoid arthritis, psoriasis, multiple sclerosis or even cancer. These diseases provoke a decrease in the quality of life and can eventually cause a reduced life span [20]. Chronic inflammatory processes are often characterized by overly activated endothelial cells and ongoing leukocyte extravasation [21]. Hence, targeting the endothelium itself and altering the leukocyte-endothelial cell interaction to prevent proceeding leukocyte infiltration into the tissue constitute valuable tools for the development of novel anti-inflammatory drugs. In fact, approved drugs like the monoclonal antibodies vedolizumab and crizanlizumab efficiently target integrins on the cell surface of leukocytes, thereby hampering the interaction of these immune cells with the endothelium [22,23]. Unfortunately, biopharmaceuticals such as monoclonal antibodies are cost-intensive and their beneficial effect may be overshadowed by, for example, anti-drug antibodies. Hence, there is an ongoing need for the evaluation of new anti-inflammatory small molecule drugs and drug leads.

The natural products harringtonine (HT) and homoharringtonine (HHT) are alkaloids from *Cephalotaxus* species that bind to the eukaryotic 60 S large ribosomal subunit, thereby altering cellular protein biosynthesis [24,25]. Both compounds have been shown to evoke profound anti-cancer effects, including apoptosis, inhibition of cell proliferation and cell cycle arrest, in various tumor cell types [26]. Semi-synthetically produced HHT, called omacetaxine mepesuccinate, has gained FDA approval for the treatment of chronic myeloid leukemia in patients who meet special criteria [27]. On top of its strong anti-cancer effects, a limited number of studies has also suggested anti-inflammatory effects of the natural product. For example, HHT has been shown to reduce inflammation in atopic dermatitis, colitis and Alzheimer's disease. In this regard, the anti-inflammatory effects of HHT have been connected to the NF-κB pathway and signal transducer and activator of transcription 3 (STAT3) signaling [28–30]. To date, no data concerning a potential anti-inflammatory action of HT are available. Although both leukocytes and the endothelium are crucially involved in the inflammatory response, previous studies on the anti-inflammatory effects of HHT mainly focused on the leukocytic site but did not investigate the role of endothelial cells. On this basis, the aim of this study was to assess the effect of the *Cephalotaxus* alkaloids HT and HHT on inflammation *in vivo* using a mouse model of peritonitis and on pro-inflammatory endothelial activation processes and the leukocyte-endothelial cell interaction *in vitro* by using human umbilical vein endothelial cells (HUVECs) as well-established model for the vascular endothelium [31].

2. Materials and methods

2.1. Compounds

HT and HHT were purchased from MedChemExpress (Monmouth Junction, NJ, USA), and cycloheximide (CHX) was obtained from Sigma-Aldrich (St. Louis, MO, USA). The p38 inhibitor SB239063 was ordered from Biomol (Hamburg, Germany). All before mentioned compounds were dissolved in DMSO to gain stock solutions. For cell culture purposes, the stock solutions were freshly diluted using cell culture medium without exceeding a final DMSO concentration of 0.1 % (v/v). Recombinant human tumor necrosis factor alpha (TNF), recombinant human interleukin-1β (IL-1β) and stromal-cell derived factor 1 (SDF-1) were obtained from PeproTech (Rocky Hill, NJ, USA).

2.2. Cell culture

Primary human umbilical vein endothelial cells (HUVECs) were prepared from umbilical veins of healthy donors (waiver W1/21 Fü has been granted for the use of anonymized human material on September 15th, 2021, issued by the head of the Research Ethics Committee/Institutional Review Board) according to the method of Jaffe et al. [32,33]. Cultivation of HUVECs was carried out in pre-coated plastic flasks (collagen G; 10 μg/ml; Biochrom, Berlin, Germany). HUVECs were split in a ratio of 1:3 and were used for experimental purposes exclusively in passage 3. The human monocytic cell line THP-1 and the human T cell line Jurkat were obtained from the German Collection of Microorganisms and Cell Cultures (DSMZ, Braunschweig, Germany). Both cell lines were cultivated in Royal Park Memorial Institute 1640 medium (RPMI; PAN-Biotech) containing 10 % FCS (Biochrom), 100 U/ml penicillin and 100 μg/ml streptomycin (PAN-Biotech) and used for experimental purposes up to passage 30. Cultivation of all cell types was performed under constant humidity at 37 °C in an atmosphere of 5 % CO_2.

2.3. Isolation of human primary leukocytes

For the isolation of human primary lymphocytes (PLs) and human primary monocytes (PMs), buffy coats from Deutsches Rotes Kreuz, Blutspendedienst Baden-Württemberg/Hessen, Institut für Transfusionsmedizin und Immunhämatologie, Frankfurt, Germany were processed based on the instructions of Bøyum [34]. In brief, plasma cells were separated by low density gradient centrifugation using lymphocyte separation medium (PromoCell, Heidelberg, Germany). The fraction containing peripheral blood mononuclear cells (PBMCs) was washed twice with ice-cold Hanks' Balanced Salt Solution (HBSS) and was then resuspended in RPMI containing 100 U/ml penicillin and 100 μg/ml streptomycin (PAN-Biotech). The cells were seeded and allowed to adhere. After 90 min, unattached PLs were separated from attached PMs

and cell culture medium was refreshed. Both cell types were cultivated for 24 h in RPMI containing 10 % FCS (Biochrom), 100 U/ml penicillin and 100 μg/ml streptomycin (PAN-Biotech) before they were used for experimental purposes.

2.4. Animal experiments

2.4.1. Animals

For the *in vivo* model of zymosan-induced peritonitis, 8–12 week-old female C57BL/6 N mice (Charles River, Sulzfeld, Germany) were used. Mice were housed on a 12 h light/dark cycle with access to food and water *ad libitum*. All behavioral studies were conducted during the light cycle of the day at room temperature (20–24 °C) by an observer blinded for the treatment of the animals.

2.4.2. Ethics approval

All experiments adhered to the Animal Research: Reporting on In Vivo Experiments (ARRIVE) guidelines and were approved by the local Animal Welfare authorities (Regierungspräsidium Darmstadt, Germany; reference number V54–19c18-FR/2026).

2.4.3. Zymosan-induced peritonitis

To induce acute peritonitis, 0.5 ml of a zymosan A suspension (Z4250, Sigma-Aldrich, Steinheim, Germany; 2 mg/ml in Dulbecco's Phosphate Buffered Saline without Ca^{2+}/Mg^{2+} (DPBS); Gibco, Darmstadt, Germany) was intraperitoneally (i.p.) administered [35,36]. Sixteen hours prior to the zymosan injection, 100 μl homoharringtonine (1 mg/kg) or vehicle (1 % DMSO in 0.9 % NaCl) was injected subcutaneously (s.c.) into the nape of the neck.

2.4.4. Dynamic weight bearing

A dynamic weight bearing (DWB) device (Bioseb, Boulogne, France) was used for non-reflexive assessment of abdominal pain in mice as described previously [36,37]. The device includes an acrylic glass cage (11 cm×11 cm) with a sensor on the floor detecting the weight borne in each limb and a camera on the top monitoring the mouse position. After habituation to the test room 1 day before the experiment, the DWB assessment was performed in naïve mice (baseline) and 5 h after the i.p. zymosan injection. For the DWB assessment, mice were placed in the test chamber, habituated for 5 min and recorded for 5 min without movement restriction. Then the mice were removed, and the test chamber was cleaned with water. The recorded weight distribution was evaluated by the DWB software as previously described [36–38]. Paw print analysis was validated manually by an observer after software evaluation. The mean over time was utilized to calculate the front paw/hind paw ratio.

2.4.5. Peritoneal lavage

After 5 h of i.p. zymosan injection, mice were deeply anesthetized by s.c. injection of 100 mg/kg ketamine and 10 mg/kg xylazine into the neck. The abdominal skin was gently incised to expose the inner peritoneum. Two milliliters of sterile, ice-cold DPBS were injected in the abdominal cavity using a 27 G needle followed by a careful manual massage for two minutes and subsequent removal of the lavage fluid with a 25 G needle mounted on a syringe. Mice were then killed by cervical dislocation while still under anesthesia. The peritoneal lavage was kept on ice, centrifuged and used for cytokine measurement and cell type analysis. FCγR (CD16/32) blocking cocktail (BD Biosciences) was added to the cells followed by an incubation with anti-I-A/I-E (anti-major histocompatibility complex II, Brilliant Violet 421-labeled, 562564), anti-CD11b (allophycocyanin, 564985), anti-Ly-6 C (lymphocyte antigen 6 complex locus C1, 560592) and anti-Ly-6 G (lymphocyte antigen 6 complex locus G, 551460); all antibodies were purchased from BD Biosciences. Cell type analysis of monocytes and neutrophils was performed using a FACSVerse flow cytometer (BD Biosciences) [39–41].

2.4.6. Cytometric bead array (CBA)

To measure the IL-1β cytokine level in the peritoneal lavage, murine IL-1β Cytometric Bead Array Flex Set (BD Biosciences) were used according to the instructions of the manufacturer. Samples were acquired with a FACSymphony A5SE spectral flow cytometer (BD Biosciences) and data was analyzed using FlowJo v10.

2.5. Cytotoxicity assays

Cytotoxicity assays were conducted to evaluate non-cytotoxic concentrations of HT and HHT for subsequent investigations regarding anti-inflammatory effects. Therefore, confluent monolayers of HUVECs were treated with HT or HHT for 24 h using the indicated concentrations followed by the measurement of cell viability (2.5.1), membrane integrity (2.5.2) and late cell apoptosis (2.5.3).

2.5.1. Cell viability assay

The metabolic activity of HUVECs was determined using the CellTiter-Blue cell viability assay (Promega, Mannheim, Germany) according to the manufacturer's instructions. In brief, 4 h before the end of the indicated treatment period the CellTiter Blue reagent was added to the cells in a ratio of 1:10. The fluorescence intensity resulting from the conversion of resazurin to resorufin was measured at 535 nm (ex) and 590 nm (em) using a microplate reader (SPECTRAFluor Plus; Tecan, Männedorf, Switzerland).

2.5.2. Lactate dehydrogenase (LDH) release

The CytoTox 96 non-radioactive cytotoxicity assay kit (Promega) was applied to measure the lactate dehydrogenase (LDH) release from HUVECs. After the indicated treatment period, an enzymatic substrate solution was added to the cell culture supernatants for 30 min. The enzymatic reaction was terminated by adding a stopping solution, and absorbance was measured at 490 nm using a Varioscan Flash microplate reader (Thermo Fisher Scientific, Schwerte, Germany). Treatment with cell lysis solution for 45 min was used as positive control for maximum LDH release into the surrounding medium.

2.5.3. Measurement of late apoptosis

Propidium iodide (PI) staining according to Nicoletti *et al.* [42] was performed to measure the percentage of late apoptotic cells in HUVECs. After the indicated treatment period, cell culture supernatants were collected and HUVECs were detached using trypsin/EDTA (Biochrom). The cells were incubated with a staining solution containing 50 μg/ml PI (Sigma-Aldrich), 0.1 % Triton X-100 (Sigma-Aldrich) and 0.1 % sodium citrate (Carl Roth, Karlsruhe, Germany) for a minimum of 2 h in the dark. Treatment with 1 μM of staurosporine (Stsp; Sigma-Aldrich) for 24 h served as positive control for the induction of apoptosis. Median values for 10,000 events per sample were recorded to determine the percentage of cells with subdiploidic DNA using a FACSVerse flow cytometer (BD Biosciences, San Jose, CA, USA).

2.6. Cell adhesion assay

2.6.1. Static cell adhesion assay

Confluent HUVECs were treated as indicated in the respective figure legend. Subsequently, THP-1 cells, Jurkat cells, PLs or PMs were fluorescence-labeled using Green CMFDA (Cayman Chemical, Ann Arbor, MI, USA), and 7.5 $\times 10^4$ (THP-1, Jurkat) or 2 $\times 10^5$ (PLs, PMs) leukocytes per well were allowed to adhere to the endothelial cell monolayer. Non-adherent leukocytes were washed off, and the relative amount of adhered fluorescence-labeled leukocytes was determined by fluorescence measurement at 485 nm (ex) and 535 nm (ex) using a microplate reader (SPECTRAFluor Plus; Tecan).

2.6.2. Cell adhesion under flow

HUVECs were seeded to channel slides (μ-Slides I Luer, 0.8 mm; ibidi

GmbH, Martinsried, Germany) and allowed to adhere for 2 h. Subsequently, the channel slides were connected to a pump system (ibidi GmbH) and a unidirectional flow (5 dyn/cm^2) was applied on the cells. After 24 h, HUVECs were pretreated with HT or HHT as indicated for 30 min followed by activation using TNF (10 ng/ml) for 24 h. THP-1 cells were fluorescence-labeled with Green CMFDA (Cayman Chemicals), and 8 $\times 10^5$ cells/ml were allowed to adhere to the endothelial cell monolayer in a unidirectional flow (0.5 dyn/cm^2). Non-adherent leukocytes were washed off, and adherent THP-1 cells were lysed using radioimmunoprecipitation assay (RIPA) lysis buffer. Fluorescence measurement was conducted at 485 nm (ex) and 535 nm (ex) using a microplate reader (SPECTRAFluor Plus; Tecan).

2.7. Transmigration assay

1 $\times 10^5$ HUVECs were grown on collagen G (10 μg/ml; Biochrom)-coated Transwell inserts (growth area 0.33 cm^2, 8 μm pore size, polycarbonate; Corning, NY, USA) for 24 h and then pretreated with HT or HHT as indicated for 30 min followed by addition of TNF (10 ng/ml) for 24 h. THP-1 cells were fluorescence-labeled with Green CMFDA (Cayman Chemicals) and 2 $\times 10^4$ THP-1 cells/well were allowed to transmigrate through the endothelial monolayer for 2 h towards an SDF-1 (500 ng/ml; PeproTech) gradient in the lower compartment of the Transwell system. Non-migrated THP-1 cells in the upper compartment were removed using a cotton swap. Transmigrated THP-1 cells were lysed using RIPA buffer and fluorescence intensity was determined at ex 485 nm and em 535 nm using a microplate reader (SPECTRAFluor Plus, Tecan).

2.8. Flow cytometry

Confluent HUVECs were treated as indicated in the respective figure legend. Subsequently, HUVECs were detached using HyClone HyQTase (GE Healthcare, Freiburg, Germany) and stained for 45 min on ice in the dark for mouse anti-human ICAM-1 (FITC, 1:33, MCA1615F; Bio Rad, Hercules, CA, USA), mouse anti-human VCAM-1 (PE, 1:20, 555647; BD Biosciences), mouse anti-human E-selectin (PE, 1:10, 551145; BD Biosciences) or mouse anti-human TNFR1 (1 μg/10^6 cells, sc8436; Santa Cruz Biotechnology, Dallas, TX, USA). In case of TNFR1 staining, cells were subsequently labeled with an Alexa Fluor 488-conjugated secondary antibody (goat anti-mouse; 1:400, A11001; Thermo Fisher Scientific) for 45 min in the dark. Protein cell surface expression was quantified by recording median values for 20,000 events per sample using a FACSVerse flow cytometer (BD Biosciences).

2.9. Quantitative real-time PCR

Confluent HUVECs were treated as indicated in the respective figure legend. Cellular RNA was isolated with the RNeasy Mini Kit (Qiagen, Hilden, Germany) according to the manufacturer's protocol. On-column DNase digestion was performed with the RNase-Free DNase Set (Qiagen). 1 μg of RNA was subsequently reverse-transcribed into cDNA using ProtoScript II reverse transcriptase (New England Biolabs Inc., Ipswich, MA, USA). Quantitative real-time PCR was performed with the SYBR Green PCR Master Mix (Life Technology, Carlsbad, CA, USA) following the comparative C_T quantitation method $2^{-\Delta\Delta Ct}$ and using a StepOnePlus System (Applied Biosystems, CA, USA). *GAPDH* served as housekeeping gene. Data were analyzed using the StepOnePlus Software v2.3. The following primer pairs were used: *ICAM1* (forward: 5'- CTG CTC GGG GCT CTG TTC-3'; reverse: 5'-AAC AAC TTG GGC TGG TCA CA-3'), *VCAM1* (forward: 5'-CCA CAG TAA GGC AGG CTG TAA-3'; reverse: 5'-GCT GGA ACA GGT CAT GGT CA-3'), *SELE* (forward: 5'-AGA TGA GGA CTG CGT GGA GA-3'; reverse: 5'-GTG GCC ACT GCA GGA TGT AT-3'), *NFKBIA* (forward: 5'-AGC TCC GAG ACT TTC GAG GA-3'; reverse: 5'-GAG TCA GGA CTC CCA CGC T-3'), IRF1 (forward: 5'-ACA AGG ATG CCT GTT TGT TCC-3'; reverse: 5'-TGG AAG CAT CCG GTA CAC TC-3'), GATA6 (forward: 5'-ACC ACC TTA TGG CGC AGA AA-3'; reverse: 5'-TCA TAG CAA GTG GTC TGG GC-3'), *GAPDH* (forward: 5'-CCA CAT CGC TCA GAC ACC AT-3'; reverse: 5'-TGA AGG GGT CAT TGA TGG CAA-3').

2.10. Western blot analysis

Confluent HUVECs were treated as indicated in the respective figure legend and subsequently lysed with RIPA lysis buffer supplemented with protease and phosphatase inhibitors. The protein content of each individual sample was detected using the Pierce BCA Protein Assay Kit (Thermo Fisher Scientific). A pyronin-based sample buffer containing sodium dodecyl sulfate (SDS) was added to the samples followed by incubation at 95 °C for 5 min. Equal amounts of protein (20–40 μg) were separated by SDS-polyacrylamide gel electrophoresis (SDS-PAGE; Bio-Rad Laboratories, Munich, Germany) and transferred onto a polyvinylidene fluoride membrane (PVDF; Bio-Rad) by semi-dry electroblotting using the Trans-Blot Turbo Transfer System (Bio-Rad) at constant voltage (25 V) for 30 min. Unspecific binding sites were blocked with 5 % non-fat dry milk (Blotto; Carl Roth) or 5 % BSA (MilliporeSigma) containing 0.1 % Tween-20 (Sigma-Aldrich) followed by primary antibody incubation. Rabbit anti-human ICAM-1 (#4915), rabbit anti-human TNFR1 (#3736), rabbit anti-human phospho-TAK1 (Thr184/187) (#4508), rabbit anti-human TAK1 (#4505), rabbit anti-human phospho-IKKα/β (#2697), rabbit anti-human IKKβ (#8943), rabbit anti-human phospho-IκBα (Ser32) (#2859), rabbit anti-human IκBα (#9242), rabbit anti-human phospho-p38 (Thr180/Tyr182) (#4511), rabbit anti-human p38 (#9212), rabbit anti-human phospho-SAPK/JNK (Thr183/Tyr185) (#4668), rabbit anti-human SAPK/JNK (#9258), mouse anti-human phospho-ERK1/2 (Thr202/Tyr204) (#9106), rabbit anti-human ERK1/2 (#9102) and rabbit anti-human IRF1 (#8478) were purchased from Cell Signaling Technologies (Leiden, Netherlands). Mouse anti-human VCAM-1 (sc13160), mouse anti-human E-selectin (sc137054), mouse anti-human IL-1R1 (sc393998), mouse anti-human GATA6 (sc517554), mouse anti-human phospho-MK2 (Thr334) (sc293139) and mouse anti-human MK2 (sc393609) were obtained from Santa Cruz Biotechnology (Heidelberg, Germany). Mouse anti-human ELAVL1 (HUR, C15200238) was purchased from Diagenode (Denville, NJ, USA). For unconjugated primary antibodies, the secondary antibodies goat anti-rabbit linked to horseradish peroxidase (HRP) (#7074) and goat anti-mouse linked to HRP (#7076) from Cell Signaling Technologies were used. For loading control, rabbit anti-human β-tubulin (#2128) from Cell Signaling Technologies, mouse anti-human topoisomerase 1 (sc271285) from Santa Cruz Biotechnology or mouse anti-human β-actin-peroxidase (A3854) from Sigma Aldrich were used. Protein expression was detected by chemiluminescence measurement and quantification of protein expression was performed by densitometric analysis of protein bands using ImageJ (software version 1.49k).

2.11. De novo protein synthesis assay

The Click-iT Plus OPP Alexa Fluor 488 Protein Synthesis Assay Kit (Thermo Fisher Scientific) was used according to the manufacturer's instructions to analyze *de novo* protein synthesis. HUVECs were seeded to 8-well μ-slides (ibidi GmbH) and treated as indicated in the respective figure legend. CHX (10 μg/ml) served as positive control for the inhibition of mRNA translation. 30 min before the treatment end point, 20 μM Click-iT *O*-propargyl-puromycin (OPP) was added to the cells leading to the incorporation of OPP into newly synthesized proteins. Cells were fixed with 4 % formaldehyde (Roti-Histofix; Carl Roth) and then permeabilized with 0.5 % Triton X-100. Copper catalyzed azide alkyne cycloaddition was performed to label the incorporated OPP with Alexa Fluor 488 picolylazide. NuclearMask Blue Stain was utilized to visualize cell nuclei. Microscopical images were obtained with a Leica DMI6000B fluorescence microscope (Leica Microsystems, Wetzlar,

Germany). The intensity of the Click-iT OPP signal in the nucleus was normalized to the intensity of the cell nuclei staining (NuclearMark Blue Stain) and analyzed using ImageJ (software version 1.49k).

2.12. Preparation of cytosolic and nuclear protein fractions

Subcellular protein fractions were prepared as described previously [32]. A pyronin-based sample buffer containing SDS was added to the samples followed by incubation at 95 °C for 10 min. Equal amounts of protein (30–40 μg) were used for western blot analysis as described in Section 2.10. Topoisomerase I and β-tubulin served as markers for the purity of the nuclear and cytosolic fraction, respectively.

2.13. Immunofluorescence staining

HUVECs were seeded to collagen G-coated 8-well μ-slides (ibidi GmbH) and treated as indicated in the respective figure legends. After the treatment end point, cells were fixed with 4 % formaldehyde (Roti-Histofix; Carl Roth) and permeabilized with 0.2 % Triton X-100. Unspecific binding sites were blocked with 0.2 % BSA (MilliporeSigma), and cells were treated with rabbit anti-human NF-κB p65 (1:400, sc8008; Santa Cruz Biotechnology) followed by incubation with an Alexa Fluor 488-conjugated secondary antibody (goat anti-mouse, 1:400, A11001; Thermo Fisher Scientific) in the dark. Immunofluorescence staining was detected using a Leica DMI6000B fluorescence microscope (Leice Microsystems) and image quantification was performed using ImageJ (software version 1.49k) allowing determination of NF-κB p65 nuclear translocation.

2.14. Polysome profiling

Polysomal fractionation was conducted as described previously [43]. In brief, confluent HUVECs were treated with TNF (10 ng/ml) alone or in combination with HHT (100 nM) for 2 h. Then, CHX (100 μg/ml) was added for 10 min to stall translation. Cells were washed with PBS containing CHX (100 μg/ml), scraped off the plates and lysed using polysome lysis buffer (140 mM KCl, 20 mM Tric-HCl pH 8.0, 5 mM $MgCl_2$, 0.5 % NP-40, 0.5 mg/ml heparin, 1 mM DTT, 100 U/ml RNasin, 100 μg/ml CHX). The cell lysate was layered on top of a sucrose gradient (10–50 %), and ultracentrifugation was performed at 35,000 rpm and 4 °C for 2 h without deceleration using a SW40 Ti rotor (Beckman Coulter, Brea, USA). For polysome fractionation (1 ml/fraction), a Gradient Station (BioComp Instruments, Fredericton, Canada) was used, and UV absorbance was measured at 254 nm (EM-1 Econo UV Monitor, Bio-Rad Laboratories). The RNA of each fraction was precipitated with 3 M sodium acetate and isopropanol over night at −20 °C. RNA was further isolated using the RNeasy Micro Kit (Qiagen) according to the manufacturer's instructions. The mRNA concentration was measured at 260 and 280 nm with a P330 nanophotometer (Implen GmbH) and then reverse-transcribed into cDNA (ProtoScript II reverse transcriptase, New England Biolabs Inc). Subsequently, RT-qPCR was performed using the StepOnePlus System (Applied Biosystems). The following primer pairs were used for qPCR: *ICAM1* (forward: 5'- CTG CTC GGG GCT CTG TTC-3'; reverse: 5'-AAC AAC TTG GGC TGG TCA CA-3'), *SELE* (forward: 5'-AGA TGA GGA CTG CGT GGA GA-3'; reverse: 5'-GTG GCC ACT GCA GGA TGT AT-3').

2.15. Statistical analysis

The number of independently performed experiments (*n*) indicates different donors for primary cells. All experiments were performed independently at least three times; the actual number of performed experiments is stated in the respective figure legend. Statistical analyses were performed using GraphPad Prism software version 10 (San Diego, USA). One-way ANOVA followed by Tukey's *post hoc* test or unpaired Student's *t*-test was used for the evaluation of significant differences. $P \leq 0.05$ was considered as statistically significant. Data are expressed as mean ± standard error of the mean (SEM).

3. Results

3.1. Homoharringtonine reduces inflammation in vivo in a murine peritonitis model

To evaluate the anti-inflammatory properties of HHT *in vivo*, we used the murine zymosan-induced peritonitis model, a widely used model for sterile inflammation [44]. Mice were s.c. treated with HHT (1 mg/kg) or vehicle (1 % DMSO in 0.9 % NaCl) 16 h prior to the i.p. injection of zymosan A. Before (baseline) and 5 h after the zymosan injection, the pain behavior was assessed using a dynamic weight bearing (DWB) device. At baseline, mice put more weight on their hind paws compared to their front paws, as expected. The zymosan injection caused a weight shift towards the front paws, indicating abdominal inflammatory pain (Fig. 1a). Interestingly, the zymosan-induced weight shift was significantly lower in HHT-treated mice as compared to vehicle-treated mice (Fig. 1a). These data suggest that HHT ameliorates abdominal inflammatory pain *in vivo*.

Investigation of the peritoneal lavage, which was obtained immediately after the DWB test 5 h post-zymosan, further revealed that HHT significantly reduced the zymosan-induced infiltration of monocytes and neutrophils to the peritoneum (Fig. 1b) and considerably lowered the concentration of the pro-inflammatory cytokine IL-1β by approximately 50 % (Fig. 1c). In sum, these data reveal that HHT has strong anti-inflammatory properties *in vivo*.

3.2. (Homo-)harringtonine hampers the leukocyte-endothelial cell interaction in vitro

As an initial step for studying the anti-inflammatory actions of HHT in endothelial cells *in vitro*, cytotoxic concentrations were evaluated and excluded from further investigations. We also included the structurally related compound harringtonine (HT) to compare effects and effect sizes of the two *Cephalotaxus* alkaloids. Treatment of HUVECs for 24 h with concentrations of up to 300 nM of HT and HHT did not influence the cell viability (Figure S1a), membrane integrity (Figure S1b) and apoptosis rate (Figure S1c). Based on these results, the effect of up to 300 nM of HT and HHT on the leukocyte-endothelial cell interaction was analyzed by focusing on the leukocyte adhesion to and transmigration through a HUVEC monolayer. Inflammatory activation of HUVECs was achieved through treatment with the pro-inflammatory cytokine TNF (10 ng/ml). It should be noted that only endothelial cells were treated with HT and HHT as well as with TNF and that the leukocytes remained untreated during the whole experiment. Both HT and HHT significantly downregulated the adhesion of the monocytic cell line THP-1 and of primary human monocytes after 24 h of co-treatment with TNF under static conditions (Fig. 2a-b). To determine if the effect of HT and HHT on cell adhesion was specific for and limited to monocytes, the adhesive capacity of the T cell line Jurkat as well as of primary lymphocytes was also examined under the same experimental conditions (Figure S2a-b). Concurringly, the adhesion of both Jurkats and primary lymphocytes was lowered, pointing out a general effect of HT and HHT on the leukocyte-endothelial cell interaction. The reduction of leukocyte adhesion appeared in all cases to be concentration-dependent with 300 nM of HT and HHT showing the strongest effects. In sum, the overall effect size on the cell adhesion of all leukocyte types tested was stronger upon HHT treatment compared to HT treatment. The actions on leukocyte cell adhesion were further confirmed in a flow system, which mimics the physiological blood flow. Both HT and HHT, at a concentration of 300 nM, almost completely blocked the TNF-induced adhesion of THP-1 cells to a monolayer of HUVECs after 24 h under flow conditions (Fig. 2c). Besides their strong effect on leukocyte adhesion, HT and HHT also strongly downregulated the transmigration of THP-1 cells

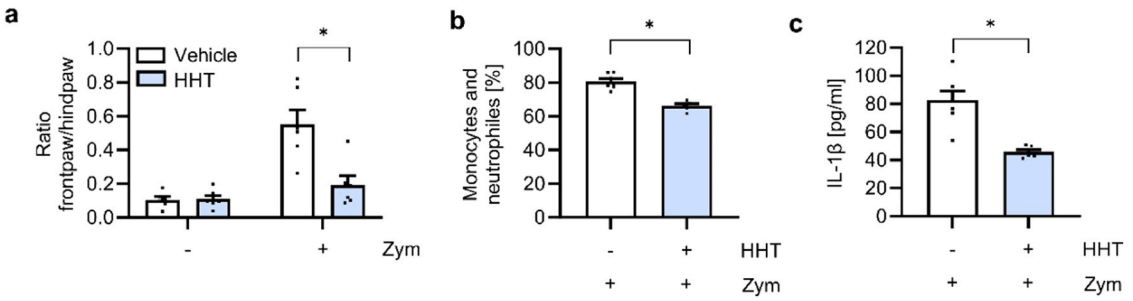

Fig. 1. Homoharringtonine reduces inflammation in a murine peritonitis model *in vivo* Mice were s.c. injected with HHT (1 mg/kg) or vehicle (1 % DMSO in 0.9 % NaCl) 16 h prior to i.p. injection of zymosan A (2 mg/ml). **a**) The weight distribution between the front paws and hind paws was assessed using a dynamic weight bearing (DWB) device at baseline and 5 h after the i.p. zymosan injection. **b**) The amount of monocytes and neutrophils in the peritoneal lavage was determined by flow cytometry. **c**) The concentration of IL-1β in the peritoneal lavage was measured by flow cytometry using a Cytometric Bead Array system. HHT, homoharringtonine; Zym, zymosan. Data are expressed as mean ± SEM. n=6 (**a**), n=5–7 (**b**), n=6–7 (**c**). *p ≤ 0.05.

through a TNF-activated monolayer of HUVECs towards an SDF-1 gradient (Fig. 2d).

3.3. (Homo-)harringtonine impacts TNF-induced expression of endothelial CAMs

The endothelial cell adhesion molecules (CAMs) ICAM-1 and VCAM-1 are instrumental in promoting firm adhesion of leukocytes to the surface of the endothelium. Hence, to explore the mechanistic basis of the reduced leukocyte-endothelial cell interaction upon HT and HHT treatment, the cellular distribution and general expression of the two CAMs were examined.

HHT provided stronger effects regarding the leukocyte-endothelial cell interaction compared to HT, therefore further experiments mainly focused on the actions of HHT. HHT significantly downregulated the cell surface expression of ICAM-1 and VCAM-1 on TNF-activated HUVECs after 24 h of treatment as determined by flow cytometry (Fig. 3a). Again, the effect was concentration-dependent with 300 nM of HHT showing the strongest decrease and an almost complete blocking of the TNF-induced CAM surface expression. In addition to affecting the CAM surface protein level, HHT also heavily impacted the total cellular protein levels of ICAM-1 and VCAM-1 in TNF-activated HUVECs after 24 h of treatment, as determined by western blotting (Fig. 3b). Hence, HHT likely influences the overall protein expression of CAMs rather than their trafficking to the cell surface.

TNF evokes a strong increase in mRNA expression of pro-inflammatory genes including CAMs. Since HHT led to a significant reduction of CAM protein expression, we next examined a potential impact on the TNF-induced mRNA expression of these CAMs. Surprisingly, while HHT indeed decreased the mRNA expression of *VCAM1* at 300 nM in TNF-activated HUVECs between 2 h to 10 h, the *ICAM1* mRNA expression was increased under the same experimental conditions (Fig. 3c). Note that HT evoked similar effects on the CAM cell surface level (Figure S3a), CAM total protein expression (Figure S3b) and *ICAM1* and *VCAM1* mRNA expression over time (Figure S3c). The effect size of HT, however, was slightly lower compared to HHT.

While ICAM-1 and VCAM-1 promote firm adhesion, selectins such as E-selectin mediate the initial rolling of leukocytes on the endothelial cell surface. HT and HHT both concentration-dependently reduced the cell surface and total protein level of E-selectin (Figure S4a-b) as well. Like for *ICAM1*, the *SELE* mRNA expression was time-dependently increased by HT and HHT in TNF-activated HUVECs (Figure S4c).

These results demonstrate, on the one hand, that the actions of HT and HHT on the leukocyte-endothelial cell interaction are probably caused by an impairment of endothelial CAMs and suggest, on the other hand, that the *Cephalotaxus* alkaloids might affect endothelial CAMs by different intracellular signaling events.

3.4. HHT increases ICAM1 mRNA levels through enhancing p38-mediated mRNA stability

ICAM1 gene transcription is strongly induced upon inflammatory activation of HUVECs. The respective mRNA, however, is highly labile and degraded quickly [45]. However, it has been shown that the mitogen-activated protein kinase p38 can prolong the *ICAM1* mRNA stability through the MK2/ELAVL1 pathway [46]. While TNF time-dependently increased p38 activation with a maximum phosphorylation after 0.5 h, which then rapidly decreased between 1 h and 4 h, additional treatment of HUVECs with HHT at 300 nM significantly increased and prolonged the TNF-mediated phosphorylation of p38 up to 2 h (Fig. 4a). Please note that this effect was only observed at concentrations of 100 nM or more of HHT (Figure S5a). Consistently, the mRNA level of *ICAM1* was only increased at concentrations of 100 nM or more, not below (Figure S5b). In general, treatment of TNF-activated HUVECs with 100 nM of HHT evoked comparable effects on the mRNA expression of *ICAM1*, *VCAM1* and *SELE* as 300 nM of HHT (Figure S5c). Since the increased and prolonged p38 activation pointed towards the possibility that HHT stabilizes the present *ICAM1* mRNA instead of increasing gene transcription, the *ICAM1* mRNA stability upon HHT treatment was examined using an mRNA decay experiment. Therefore, HUVECs were treated with TNF for 2 h to induce *ICAM1* gene transcription. Then, actinomycin D alone or in combination with HHT was added to the cells for increasing time periods between 0.5 h and 16 h, and the relative *ICAM1* mRNA expression over time was assessed. Actinomycin D is widely used to prevent new mRNA transcription and determine mRNA half-lives [47]. Actinomycin D treatment led to a rapid decrease in *ICAM1* mRNA levels, while the addition of HHT delayed actinomycin D-induced *ICAM1* mRNA degradation (Fig. 4b). To further substantiate the role of p38 in HHT-evoked stabilization of *ICAM1* mRNA expression, HUVECs were additionally treated with the p38 inhibitor SB239063, and relative *ICAM1* mRNA levels after 4 h were evaluated. While SB239063 did not alter the TNF-mediated mRNA expression of *ICAM1* after 2 h to 4 h, the increased expression in HUVECs treated with TNF in combination with 100 nM or 300 nM of HHT was significantly reduced by SB239063 (Fig. 4c, Figure S5d).

To explore the mechanistic basis of the p38-mediated *ICAM1* mRNA stabilization, western blotting was performed to analyze phosphorylation of the downstream kinase MK2. Again, HHT strongly enhanced and extended the TNF-induced phosphorylation of MK2 up to 2 h (Fig. 4d), while the p38 inhibitor SB239063 significantly lowered the HHT-induced phosphorylation of MK2 after 0.5 h to 1 h (Fig. 4e). Activated MK2 promotes the binding of ELAVL1, which is mainly located in the nucleus when inactive, to its nuclear export factor. This leads to an increased abundance of ELAVL1 in the cytosol, where it binds to AU-rich elements of the mRNA, thereby increasing stability. While TNF alone only marginally influenced the cytosolic localization of ELAVL1, HHT

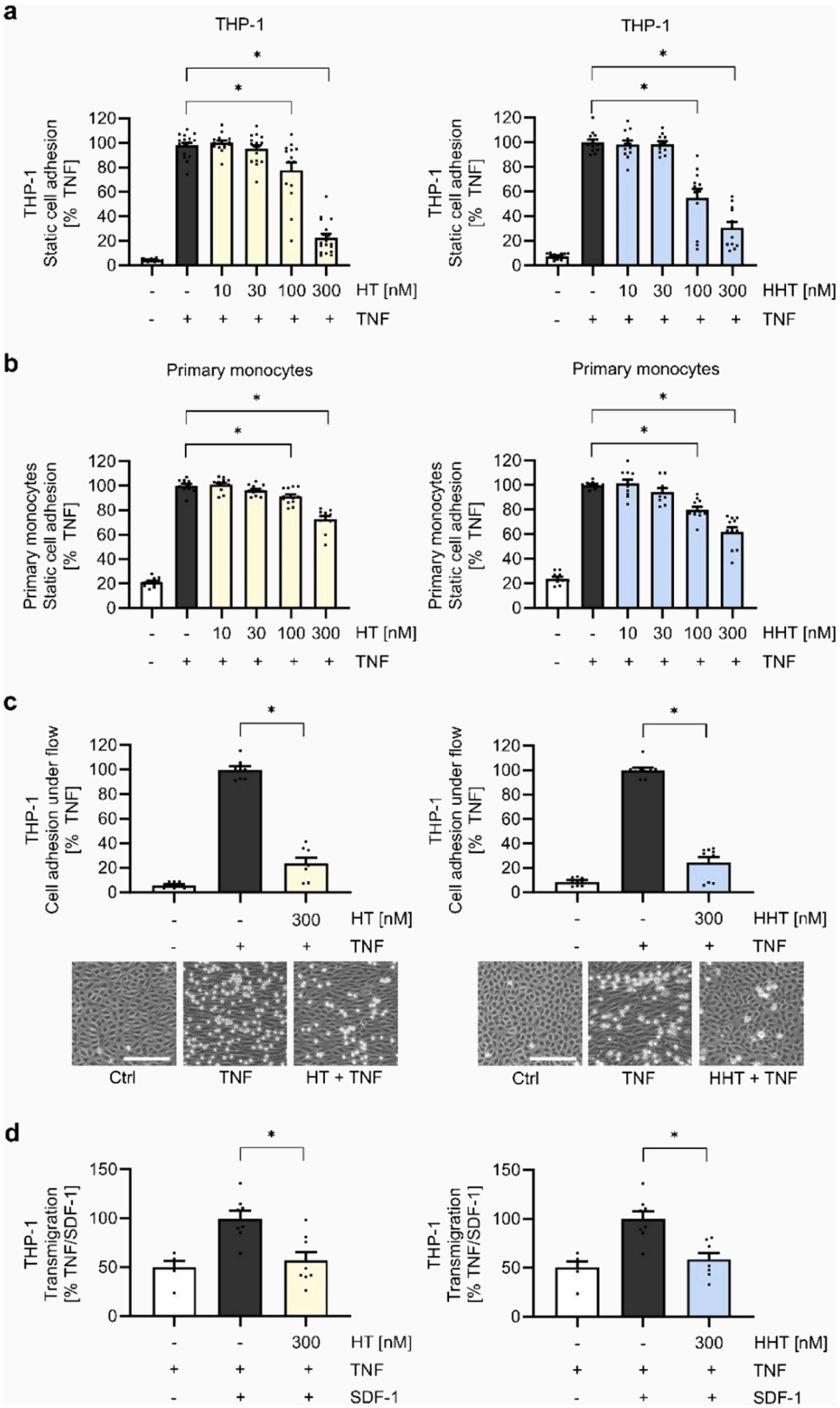

Fig. 2. HT and HHT hamper the leukocyte-endothelial cell interaction *in vitro*. **a-c**) Confluent HUVECs were pretreated with HT or HHT as indicated for 30 min followed by activation with TNF (10 ng/ml) for 24 h. Fluorescence-labeled THP-1 cells (**a**, **c**) and primary monocytes (PMs, **b**) were allowed to adhere to the HUVEC monolayer under static (**a**-**b**) or flow (**c**) conditions. Leukocyte cell adhesion was determined by fluorescence measurement. **c**) Representative images of one experiment are shown. Scale bar, 200 μm. **d**) HUVECs were grown on Transwell inserts, pretreated with HT or HHT as indicated for 30 min and activated with TNF (10 ng/ml) for 24 h. Fluorescence-labeled THP-1 cells were allowed to transmigrate through the HUVEC monolayer towards an SDF-1 gradient (500 ng/ml) for 2 h. Transmigrated THP-1 cells were quantified by fluorescence measurement. HT, harringtonine; HHT, homoharringtonine. Data are expressed as mean ± SEM. n=3 (**a** PMs, **b**, **c**), n=4 (**a** THP-1). *p ≤ 0.05.

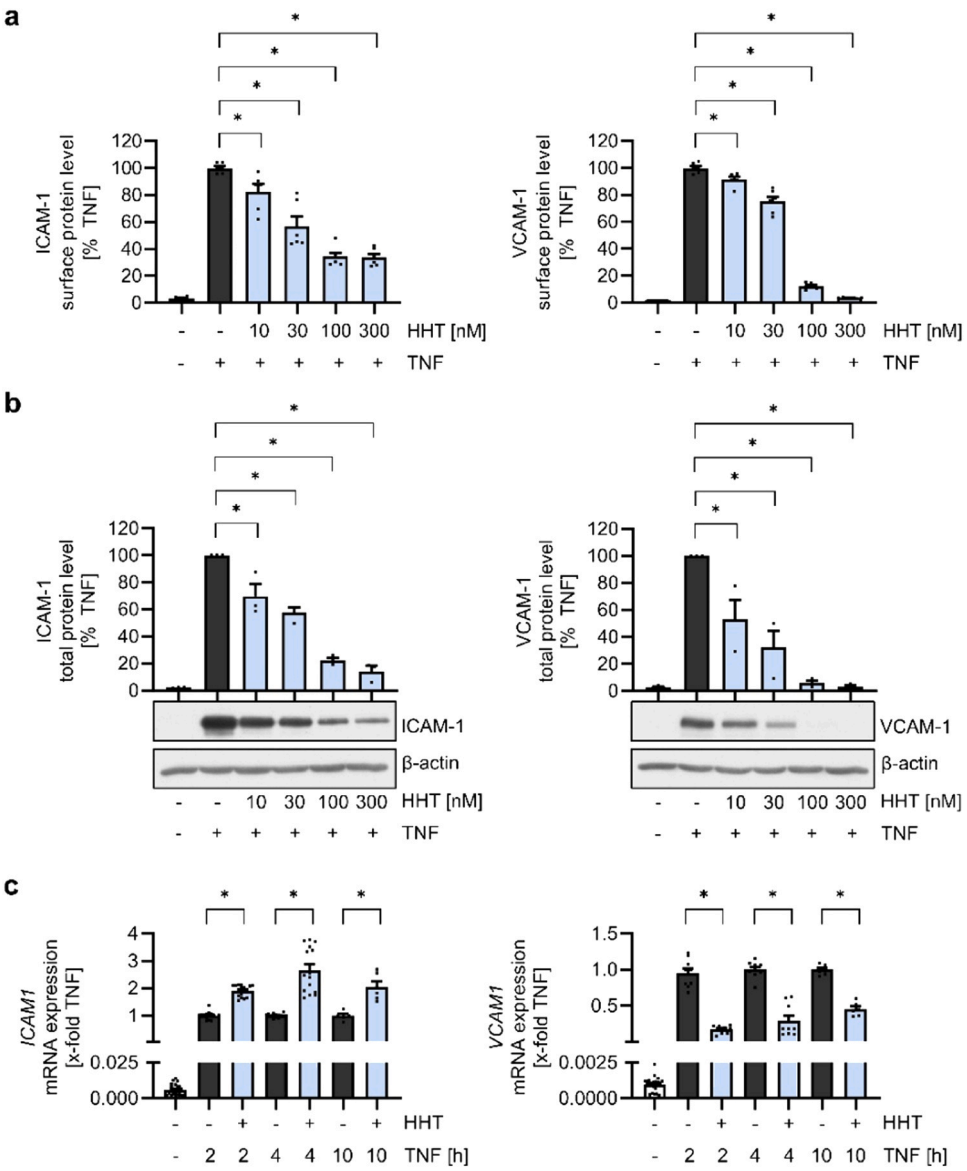

Fig. 3. HHT affects TNF-induced expression of endothelial CAMs involved in the firm adhesion of leukocytes. **a**-**b**) Confluent HUVECs were pretreated with the indicated concentrations of HHT for 30 min followed by activation with TNF (10 ng/ml) for 24 h. **a**) ICAM-1 and VCAM-1 cell surface protein expression were measured by flow cytometry. **b**) Total protein expression of ICAM-1 and VCAM-1 was detected by western blot analysis. One representative blot is shown. **c**) Confluent HUVECs were pretreated with HHT as indicated for 30 min followed by co-treatment with TNF (10 ng/ml) as indicated. The mRNA expression of *ICAM1* and *VCAM1* was analyzed by quantitative PCR. HHT, homoharringtonine. Data are expressed as means ± SEM. n=3. *p ≤ 0.05.

(300 nM) gradually enriched ELAVL1 in the cytosol up to 4 h (Fig. 4f). Simultaneously, the total protein levels of ELAVL1 remain unaffected (Fig. 4g). Again, when HUVECs were additionally incubated with SB239063, the HHT-evoked accumulation of cytosolic ELAVL1 between 2 h to 4 h was abolished (Fig. 4h).

Taken together, these results clearly demonstrate that HHT increases the TNF-induced *ICAM1* mRNA levels through the p38-/MK2-/ELAVL1-mediated stabilization of the *ICAM1* mRNA.

3.5. HHT decreases ICAM-1 protein levels through directly targeting ICAM1 mRNA translation

In various cancer cells, which often display increased protein biosynthesis, HHT influences mRNA translation through inhibiting the process of translation elongation. Consistently, by performing a protein translation assay with click chemistry, we found that after 1 h of treatment with HHT (300 nM) protein biosynthesis in HUVECs was significantly reduced to approx. 50 % (Fig. 5a). This effect on the *de novo* protein biosynthesis lasted up to 24 h of HHT treatment. Cycloheximide (CHX), a well-established translation inhibitor used as control, evoked similar effects in this experimental setup. The results suggest that HHT could directly impair the translation of *ICAM1* mRNA into the respective protein. To confirm this hypothesis, polysomes of HUVECs treated with TNF alone or in combination with HHT were fractionated and subjected to UV profiling. As shown in Fig. 5b, cotreatment of HHT (100 nM) with TNF strongly increased the relative amount of mRNA bound to monosomes (fraction 1–3) compared to TNF-treatment alone. At the same time, the relative amount of mRNA bound to late polysomes (fraction 7–10), which mainly contain mRNA that is actively translated, was significantly lowered. HHT showed no effect on the mRNA bound to early polysomes in fraction 4–6 (Fig. 5b left and middle panel). To focus on the *ICAM1* mRNA distribution across the gradients, RT-qPCR was conducted. Combined treatment of HHT and TNF strongly shifted the *ICAM1* mRNA from late polysomes to monosomes (Fig. 5b right panel).

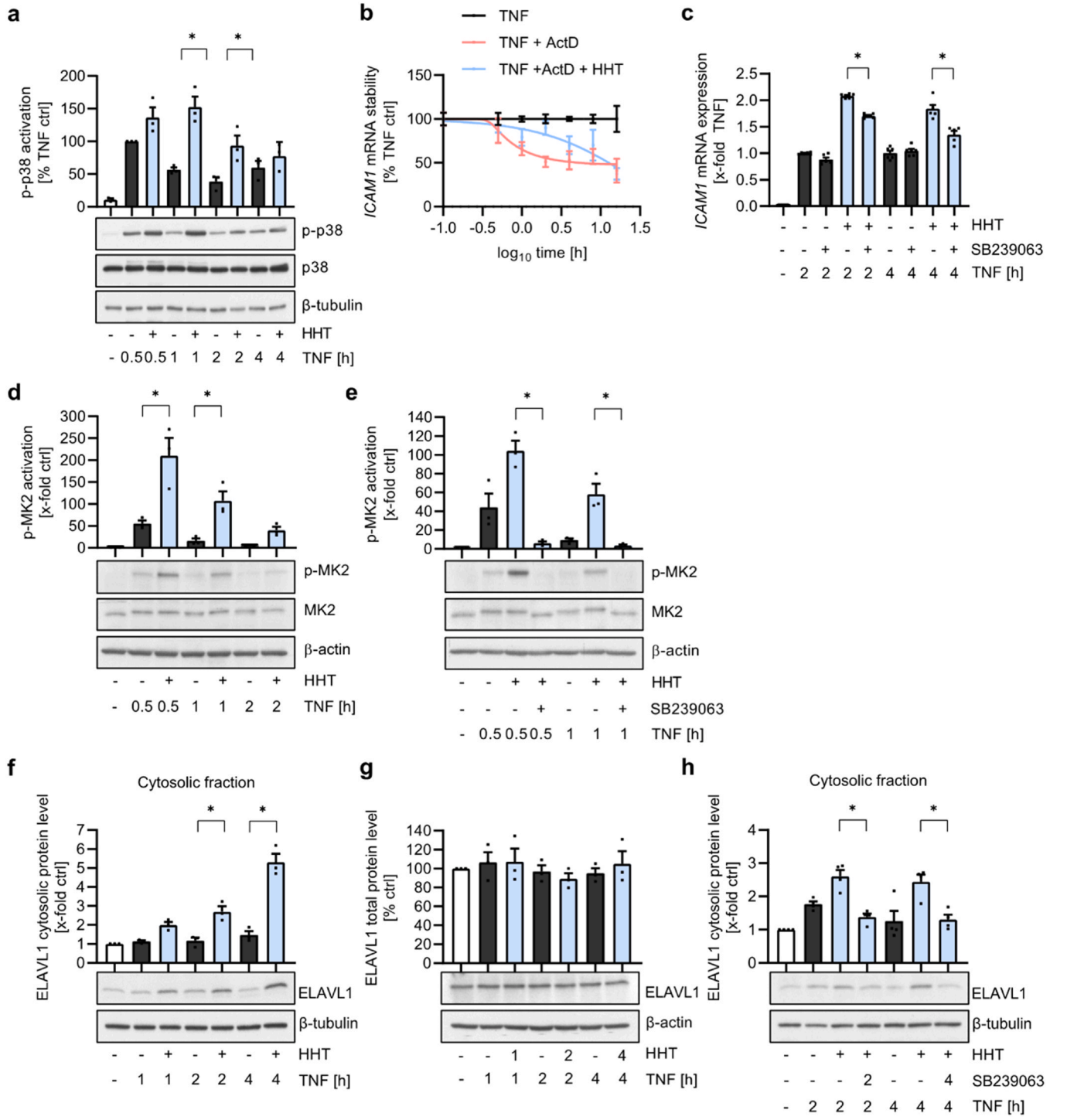

Fig. 4. HHT increases *ICAM1* mRNA stability by influencing the p38/MK2/ELAVL1 axis. **a**) Confluent HUVECs were pretreated with HHT (300 nM) for 30 min followed by co-treatment with TNF (10 ng/ml) for the indicated time points. Total protein expression of phospho-p38 (p-p38) was determined by western blot analysis. **b**) Confluent HUVECs were pretreated with TNF (10 ng/ml) for 2 h followed by the addition of actinomycin D (2 μg/ml) alone or in combination with HHT (300 nM) for the indicated time points. mRNA expression of *ICAM1* in relation to TNF treatment alone was analyzed by RT-qPCR. **c**) Confluent HUVECs were pretreated with SB239063 (10 μM) for 30 min followed by the addition of HHT (300 nM) for 30 min and subsequent co-treatment with TNF (10 ng/ml) for the indicated time points. *ICAM1* mRNA expression was determined by RT-qPCR. **d**) Confluent HUVECs were pretreated with HHT (300 nM) for 30 min followed by co-treatment with TNF (10 ng/ml) for the indicated time points. Phospho-MK2 (p-MK2) total protein level was analyzed by western blotting. **e**) Confluent HUVECs were pretreated with SB239063 (10 μM) for 30 min followed by the addition of HHT (300 nM) for 30 min and subsequent co-treatment with TNF (10 ng/ml) for the indicated time points. Phospho-MK2 (p-MK2) total protein level was determined by western blot analysis. **f-g**) Confluent HUVECs were pretreated with HHT (300 nM) for 30 min followed by activation with TNF (10 ng/ml) as indicated. ELAVL1 cytosolic (**f**) and total cellular (**g**) protein levels were determined by western blot analysis. **h**) Confluent HUVECs were pretreated with SB239063 (10 μM) for 30 min followed by addition of HHT (300 nM) for 30 min and subsequent co-treatment with TNF (10 ng/ml) as indicated. ELAVL1 cytosolic protein level was analyzed by western blotting. Representative blots are shown. HHT, homoharringtonine. Data are expressed as mean ± SEM. n=3 (**a-g**), n=4 (**h**). *$p \leq 0.05$.

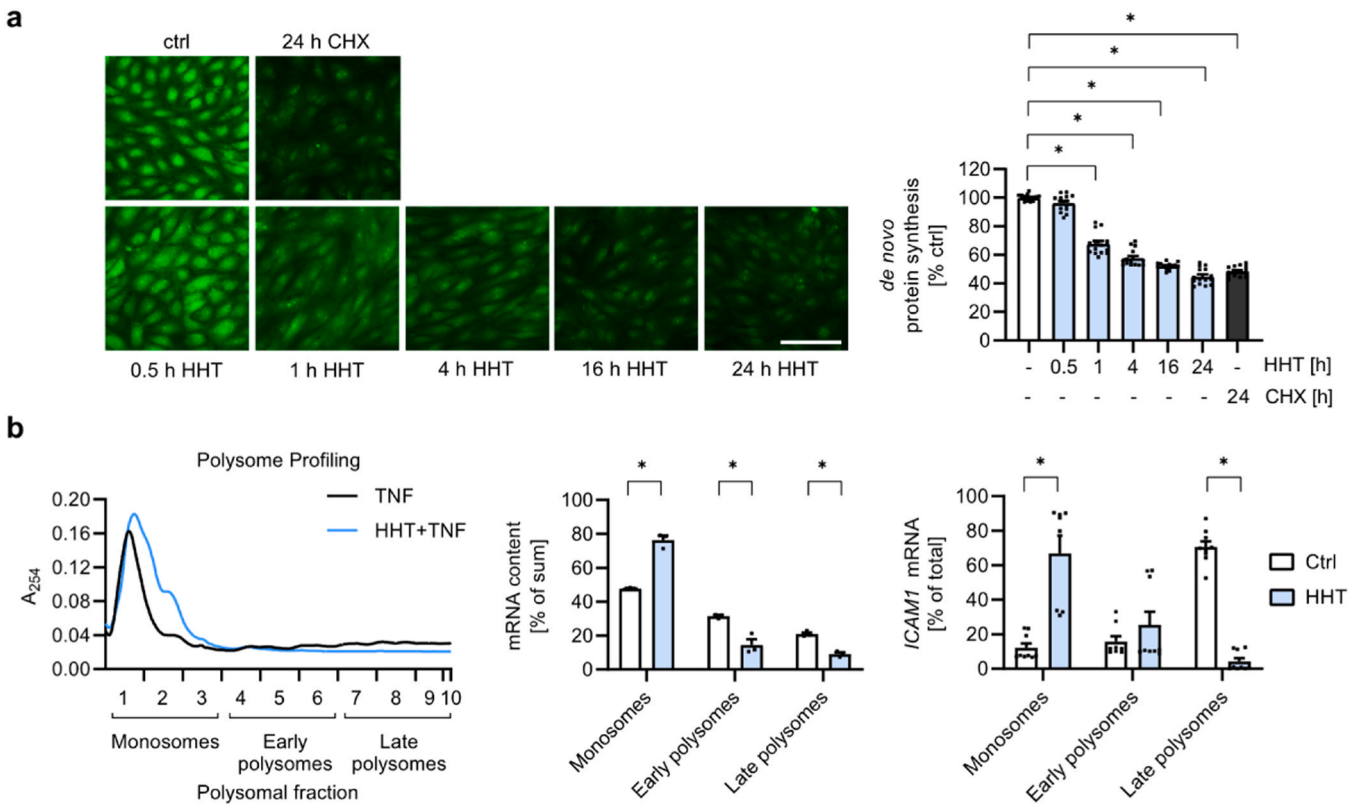

Fig. 5. HHT reduces active protein biosynthesis of ICAM-1 in HUVECs. **a**) Confluent HUVECs were treated with HHT (300 nM) as indicated. Cycloheximide (10 μg/ml, CHX) treatment was used as positive control for the inhibition of protein biosynthesis. Analysis of *de novo* protein biosynthesis was performed by immunofluorescence staining using he Click-iT Plus OPP Alexa Fluor 488 assay kit. Representative images are shown. Scale bar, 100 μm. **b**) Confluent HUVECs were treated with TNF (10 ng/ml) alone or in combination with HHT (100 nM) for 2 h. Protein translation elongation was halted using cycloheximide (100 μg/ml), and fractionation of polysomal fractions was conducted. UV absorbance of each fraction was measured at 254 nm. One representative polysome profile is shown (left). Measurement of RNA concentrations was performed using a P330 nanophotometer at 260 nm and 280 nm (middle). *ICAM1* mRNA distribution across polysomal fractions was analysed by RT-qPCR (right). HHT, homoharringtonine. Data are expressed as mean ± SEM. n=3. *p ≤ 0.05.

Again, no effect of HHT on the mRNA distribution in fraction 4–6 (early polysomes) was observed. Comparable results were also obtained regarding the mRNA distribution of *SELE* across the polysomal fractions (Figure S6).

In summary, these data indicate that HHT almost completely blocks *ICAM1* mRNA translation, while general *de novo* protein biosynthesis in HUVECs is only reduced to approx. 50 %.

3.6. Reduced VCAM1 mRNA levels are not due to an influence of HHT on NF-κB signaling

While HHT led to a stabilization of *ICAM1* mRNA levels in TNF-treated HUVECs, *VCAM1* mRNA expression was strongly reduced. Hence, we next evaluated the underlying mechanism of the reduced *VCAM1* mRNA level. The most crucial intracellular pathway for TNF-mediated pro-inflammatory actions, including mRNA expression of pro-inflammatory genes, is the NF-κB signaling. Hence, we hypothesized that an impairment of the NF-κB signaling by HHT was the cause of the decrease in *VCAM1* mRNA levels. Investigations towards the cell surface and total protein expression of the TNFR1 itself revealed a marginal reduction upon treatment with HHT at concentrations between 100 and 300 nM compared to the control treatment (Fig. 6a-b). Further assessment of the downstream NF-κB signaling pathway pointed out that HHT neither prevented the activation of the kinases TAK1 and IKKα/β (Fig. 6c-d) nor hampered IκBα protein degradation (Fig. 6e). In contrast, HHT in combination with TNF even delayed the recovery of the IκBα protein level compared to TNF treatment alone, although the respective mRNA expression of *NFKBIA* was significantly enhanced at the same time (Fig. 6f). These data suggest that HHT suppresses the new translation of the IκBα protein rather than triggering the degradation of IκBα protein. While degradation of the inhibitory protein IκBα liberates the NF-κB subunits in the cytosol by unmasking their nuclear localization sequence (NLS), binding of the NF-κB subunits to their nuclear import proteins also represents a crucial part of the nuclear translocation process. Hence, a direct influence of HHT on the nuclear translocation of the NF-κB subunit p65 was investigated. While TNF treatment strongly enhanced the nuclear translocation of p65 compared to untreated control cell, HHT was not able to reduce these TNF-evoked effects (Fig. 6g).

Importantly, when IL-1β instead of TNF was used for a pro-inflammatory activation of HUVECs, HHT evoked comparable concentration-dependent effects on the cell adhesion of THP-1 cells (Figure S7a) as well as the VCAM-1 surface protein expression (Figure S7b), total protein level (Figure S7c) and *VCAM1* mRNA expression (Figure S7d). At the same time, in line with the results on TNFR1, HHT showed no influence on the total protein level of the IL-1β cell surface receptor IL-1R1 (Figure S7e), which also induces the NF-κB signaling pathway.

Overall, these data strongly suggest that HHT does not influence *VCAM1* mRNA expression through impairment of the upstream NF-κB signaling pathway.

3.7. HHT decreases VCAM1 mRNA levels through impairing the transcription factor IRF-1

The promotor regions of *ICAM1* and *VCAM1* both contain binding motifs for the transcription factor NF-κB [18,48]. Additional binding

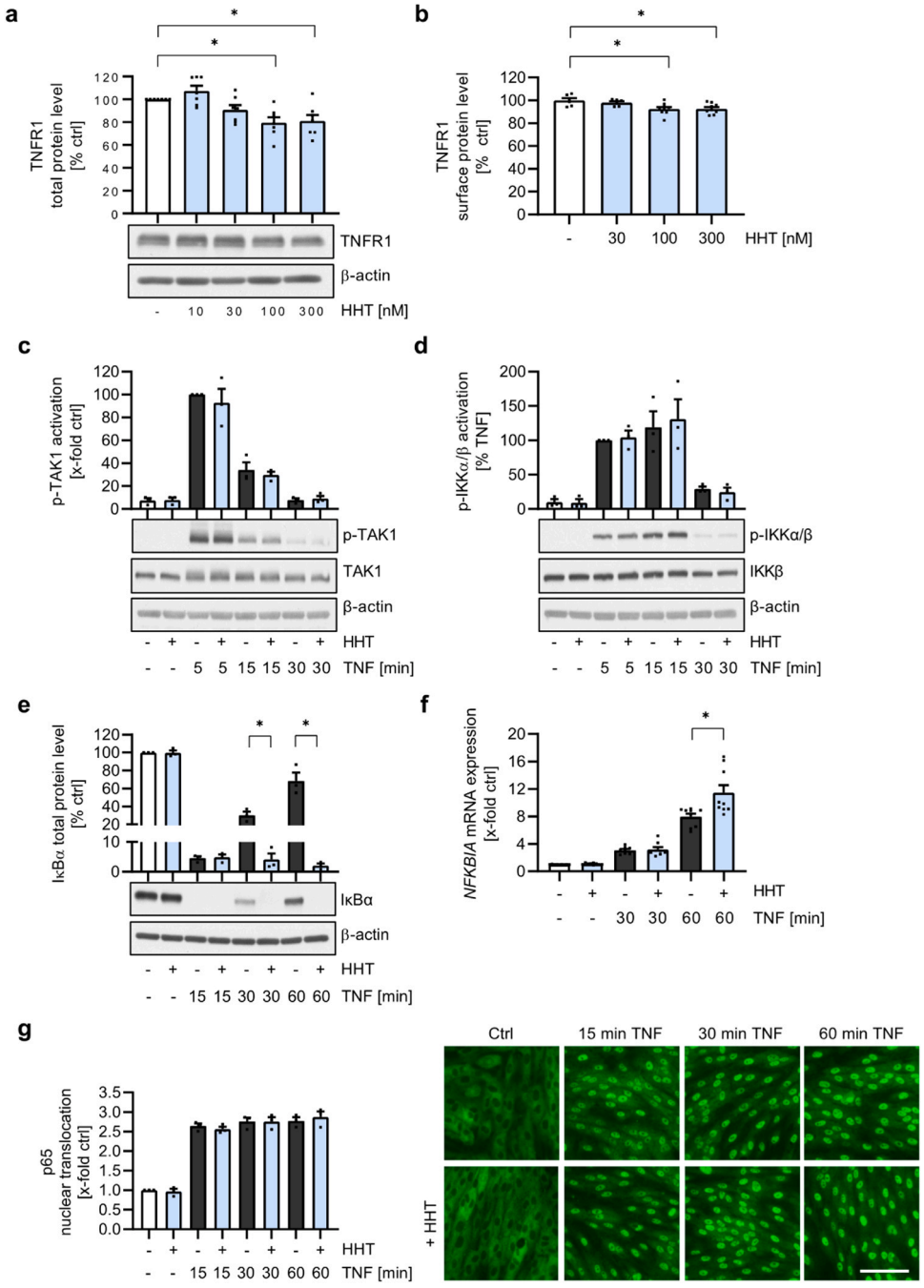

Fig. 6. HHT does not influence NF-κB signaling to reduce VCAM1 mRNA levels. **a**-**b**) Confluent HUVECs were treated with indicated concentrations of HHT for 30 min. **a**) Total protein expression TNFR1 was analyzed by western blot experiments. One representative blot out is shown. **b**) TNFR1 cell surface expression was measured by flow cytometry. **c**-**g**) Confluent HUVECs were pretreated with HHT (300 nM) for 30 min followed by cotreatment with TNF (10 ng/ml) for the indicated time points. Total protein expression of phospho-TAK1 (p-TAK1, **c**), phospho-IKKα/β (p- IKKα/β, **d**) and IκBα (**e**) was detected by western blot analysis. One representative blot is shown. Total mRNA expression of *NFKBIA* (**f**) was detected by quantitative PCR. **g**) The nuclear translocation of p65 was determined by immunofluorescence staining. Representative images are shown. Scale bar, 100 μm. HHT, homoharringtonine. Data are expressed as means ± SEM. n=4 (**a**), n=3 (**b**-**g**). *p ≤ 0.05 vs. negative control (**a**-**b**) or TNF control (**e**-**f**).

motifs, however, vary with the promotor region of *VCAM1* but not *ICAM1* also including IRF-1 and GATA-6 binding domains. Considering that HHT did not influence TNF-dependent NF-κB activation, a potential connection of HHT to the transcription factors IRF-1 and GATA-6 was evaluated. Regulation of IRF-1 expression and IRF-1-dependent gene expression is, amongst others, mediated through mitogen activated protein kinases (MAPK) including JNK, p38 and ERK, since they alter the active transcription of *IRF1* mRNA [49]. HHT induced the phosphorylation-dependent activation of the MAPK p38 (Fig. 4a), hence we next addressed a potential induction of the other MAPKs JNK and ERK by HHT. Indeed, HHT showed a reinforcing and prolonging effect on the TNF-induced activation of JNK between 0.5 h and 2 h (Fig. 7a). While TNF alone did not induce the phosphorylation of ERK1/2 to any extent, additional HHT treatment strongly and ongoingly mediated the activation of ERK1/2 between 0.5 h to 4 h (Fig. 7b). Overall, this inducing activity of HHT on the MAPKs JNK and ERK, as seen also for p38, was only observed at concentrations of 100 nM or higher (Figure S8a-b). To address if, through MAPK activation, HHT

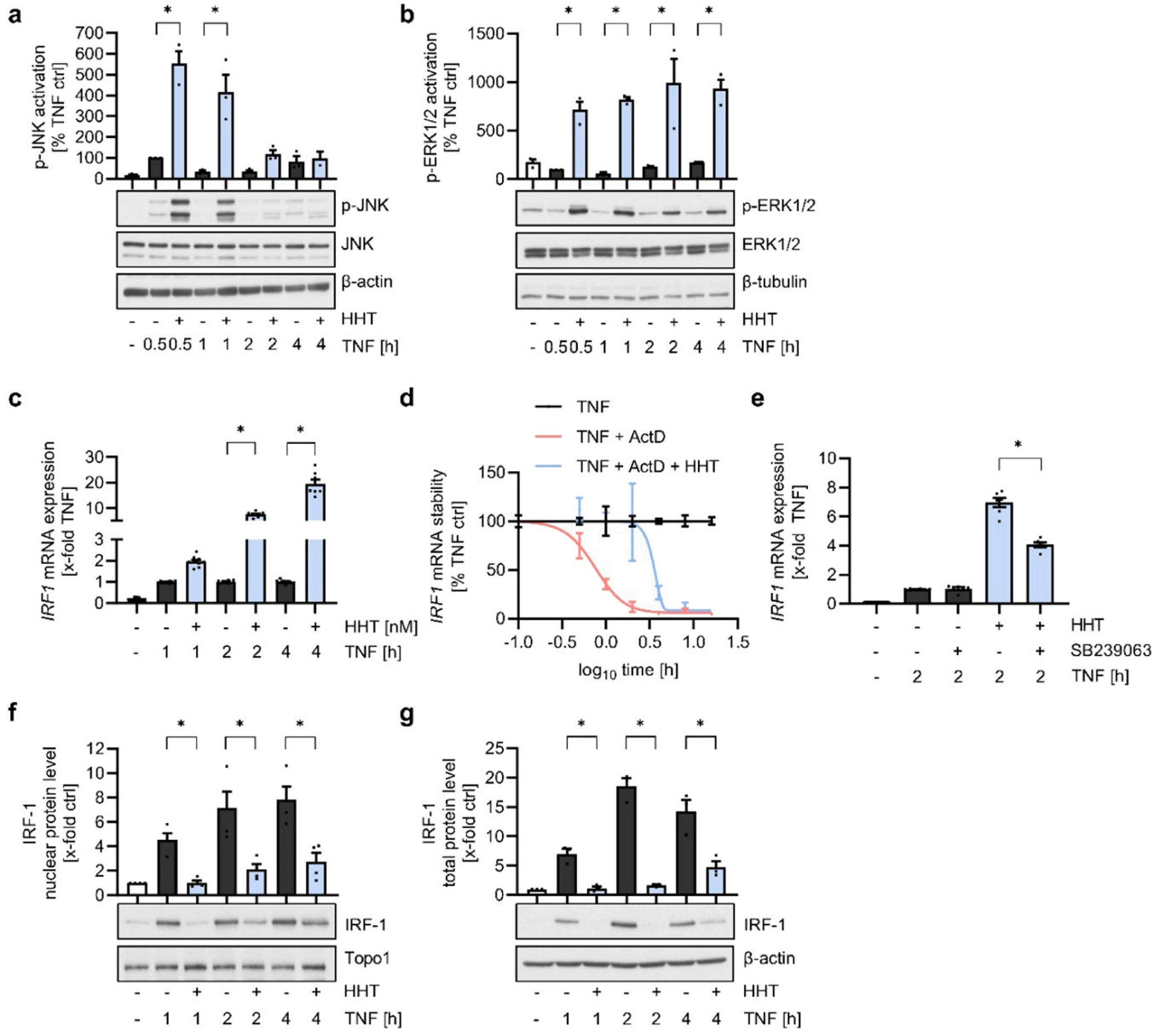

Fig. 7. HHT reduces VCAM1 mRNA expression by influencing IRF-1. **a-c**) Confluent HUVECs were pretreated with HHT (300 nM) for 30 min followed by co-treatment with TNF (10 ng/ml) as indicated. Total protein expression of phospho-JNK (p-JNK, **a**) and phospho-ERK1/2 (p-ERK1/2, **b**) was determined by western blot. *IRF1* mRNA expression (**c**) was measured by RT-qPCR. **d**) Confluent HUVECs were pretreated with TNF (10 ng/ml) for 2 h followed by the addition of actinomycin D (2 μg/ml) alone or in combination with HHT (300 nM) for the indicated time points. mRNA expression of *IRF1* in relation to TNF treatment alone was analyzed by RT-qPCR. **e**) Confluent HUVECs were pretreated with SB239063 (10 μM) for 30 min followed by the addition of HHT (300 nM) for 30 min and subsequent co-treatment with TNF (10 ng/ml) as indicated. *IRF1* mRNA expression was determined by RT-qPCR. **f-g**) Confluent HUVECs were pretreated with HHT (300 nM) for 30 min followed by co-treatment with TNF (10 ng/ml) for the indicated time points. IRF-1 nuclear (**f**) and total cellular (**g**) protein levels were determined by western blot. Representative images are shown. HHT, homoharringtonine. Data are expressed as mean ± SEM. n=3. *p ≤ 0.05.

destabilizes *IRF1* mRNA levels, its mRNA expression was evaluated. RT-qPCR experiments, however, revealed that HHT in combination with TNF treatment increased rather than decreased the mRNA level of *IRF1* over a period of 4 h compared to TNF alone (Fig. 7c). Considering that *ICAM1* mRNA levels were increased due to stabilization of the already build mRNA and not because of an increased mRNA transcription, mRNA decay experiments were performed for *IRF1* mRNA. Indeed, the experimental results confirmed that HHT strongly elevated the mRNA stability of *IRF1* (Fig. 7d). Like for *ICAM1*, this effect was mediated by p38, since the p38 inhibitor SB239063 significantly reduced *IRF1* mRNA levels in HUVECs treated with a combination of HHT and TNF (Fig. 7e).

IRF1 mRNA and IRF-1 protein expression are rapidly increased after pro-inflammatory activation of cells. After successful mRNA translation in the cytosol, IRF-1 translocates to the nucleus where it binds to the promotor regions of downstream target genes. Hence, although HHT did not impair *IRF1* gene transcription, a potential influence on the nuclear translocation of IRF-1 as root cause for the reduced *VCAM1* mRNA levels was supposed. Indeed, cell fractionation followed by western blot analysis demonstrated that the nuclear protein level of IRF-1 was significantly reduced in TNF-activated HUVECs when additionally treated with HHT (Fig. 7f). To explore the underlying mechanism leading to the reduced abundance of IRF-1 in the nucleus, we evaluated if HHT influences the IRF-1 total protein level and therefore also the nuclear abundance or if HHT actively prevents the nuclear translocation of IRF-1. Western blot analysis of the IRF-1 protein level in total cell lysates corroborated that through preventing the total protein

expression also the nuclear abundance of IRF-1 was reduced by HHT (Fig. 7g). Surprisingly, while HHT showed similar time-dependent effect on the *GATA6* mRNA level compared to *IRF1* (Figure S8c), neither the presence of GATA-6 in the nuclear fraction (Figure S8d) nor the total protein level of GATA-6 were influenced at all by HHT (Figure S8e). Collectively, these data show that HHT prevents *VCAM1* mRNA expression in an IRF-1-dependent but GATA-6-independent way.

4. Discussion

Since their discovery, harringtonine (HT) and homoharringtonine (HHT), plant-derived natural products and inhibitors of translation elongation, have been extensively studied regarding their anti-cancer properties *in vitro* and *in vivo*. Homoharringtonine obtained approval by the FDA for the treatment of chronic myeloid leukemia in patients who are resistant and/or intolerant to two or more tyrosine kinase inhibitors [26]. Besides, also actions of HHT in the field of allergic and Alzheimer's disease-related inflammation have been reported [28,29]. In this context, however, studies have mainly focused on immune cells and have neglected the role of HHT in endothelial cells, which are key players in inflammatory processes. For HT, no anti-inflammatory actions have been uncovered to date.

In the present study, we evaluated the anti-inflammatory potential of the *Cephalotaxus* alkaloids HT and HHT *in vivo* and *in vitro*. In the well-established zymosan-induced peritonitis model, we found that HHT provides strong anti-inflammatory effects *in vivo*: On the one hand, the immune cell infiltration of monocytes and neutrophils was lowered, on the other hand, the cytokine secretion of IL-1β was hampered. These anti-inflammatory properties were accompanied by a significant reduction of the peritonitis-associated abdominal pain behavior. To our knowledge, this is the first study providing evidence that HHT inhibits inflammatory pain behavior.

Immune cell infiltration heavily relies on the interaction between leukocytes and the endothelium. The endothelium thereby mediates the extravasation of the immune cells from the blood to the underlying damaged tissue. Hence, in further *in vitro* studies, we focused on the effects of HT and HHT on the leukocyte-endothelial cell interaction. In accordance with the effects observed on the immune cell infiltration *in vivo*, HHT also significantly decreased the adhesion of different types of primary leukocytes (PMs, PLs) and leukocyte cell lines (THP-1, Jurkat) to endothelial cells and furthermore lowered the transmigration of THP-1 cells through an endothelial monolayer. Interestingly, studies in hepatocarcinoma cells have outlined varying effects of HT and HHT on the cell cycle distribution, with HT increasing the percentage of cells in the S-phase while lowering the percentage of cells in the G_2/M-phase and HHT increasing the percentage of cells in the G_2/M-phase while lowering the percentage of cells in the G_0/G_1-phase [50]. Thus, coinciding effects of the two compounds cannot be automatically assumed. Nevertheless, in this study, HT treatment influenced the leukocyte adhesion cascade in a comparable way as HHT; the effect size, however, remained lower. These findings are in accordance with previous studies outlining a greater effect of HHT on the colony formation of tumor cells than of HT [51]. Importantly, in all these *in vitro* models, solely endothelial cells were treated with HT or HHT, while leukocytes remained untreated. Hence, both *Cephalotaxus* alkaloids provided specific anti-inflammatory effects on endothelial cells that led to a reduced leukocyte adhesion and transmigration. In this regard, HT and HHT affected endothelial cells through reducing the cell surface and total protein expression of CAMs (E-selectin, ICAM-1, VCAM-1) that are crucial for the leukocyte rolling on and firm adhesion to the endothelium. While other inhibitors of protein biosynthesis like narciclasine or vioprolide A have been shown to reduce the mRNA expression of both *ICAM1* and *VCAM1* [32,36], demonstrating a general influence on the transcription of these pro-inflammatory genes, this was not the case for HT and HHT. In contrast, HT and HHT strongly elevated *ICAM1* mRNA levels while significantly reducing *VCAM1* mRNA expression. These data suggested that HT and HHT prevent CAM expression through distinct pathways.

Considering that the overall treatment effect of HHT on the leukocyte-endothelial cell interaction and CAM expression was stronger than that of HT, further experiments regarding the underlying mechanistic were mainly carried out for HHT. Previous studies have demonstrated that mRNAs containing AU-rich elements (ARE), including many pro-inflammatory mediators and proteins like CAMs, are highly susceptive to rapid degradation [52]. Nevertheless, these AREs can be masked by RNA-binding proteins, thereby enhancing mRNA stability. One important axis through which the stability of mRNAs with AREs is increased, consists of the p38/MK2/ELAVL1 pathway, with ELAVL1 being the RNA-binding protein that masks the ARE of the mRNA [53]. The mitogen-activated protein kinase p38, in turn, has been linked to the so-called ribotoxic stress response, which occurs when specific regions of the 28 S ribosomal RNA become occupied. This leads to a ZAKα dependent activation of p38, JNK and ERK [54,55]. Considering that HHT has been described as inhibitor of translation elongation in different cell types and has been found to bind to the A-site of the 60 S ribosomal subunit in *Saccharomyces cerevisiae*, a mechanism of ribotoxic stress-induced p38 activation and subsequent mRNA stabilization seemed plausible [56]. Indeed, we could show that HHT significantly enhanced and extended the TNF-induced phosphorylation of p38 at concentrations of 100 nM or higher. This activation of p38 led to an activation of the downstream kinase MK2 through which the cytosolic level of ELAVL1 was significantly elevated, resulting in a stabilization of *ICAM1* mRNA. Importantly, at the same time neither MK2 nor ELAVL1 total protein level was altered by HHT. Bearing in mind that HHT reduces protein biosynthesis in different cells, we monitored the incorporation of OPP into newly synthesized proteins in HUVECs and verified that HHT reduces the *de novo* protein synthesis also in endothelial cells. Polysome profiling further confirmed that – despite elevated *ICAM1* mRNA levels – the mRNA translation into ICAM-1 protein was specifically affected by HHT. This effect occurred through shifting the *ICAM1* mRNA distribution from late, actively polysomes to monosomes.

While the influence of HHT on ICAM-1 protein expression could be solely explained by an inhibition of protein biosynthesis, VCAM-1 was also affected on the mRNA level. In our study, we primarily used TNF as pro-inflammatory cytokine. TNF acts through binding to its cell surface receptor TNFR1. In the following, intracellular NF-κB signaling is initiated leading to enhanced pro-inflammatory gene expression. Over the last years, various inhibitors of mRNA translation have been identified to exert anti-inflammatory actions through influencing either TNFR1 expression itself or hampering downstream NF-κB signaling. While some inhibitors of protein biosynthesis influence the expression of TNFR1 directly, such as the plant-derived compound narciclasine or the myxobacterial product vioprolide A, other translation inhibitors, including mycotrienin II and cytotrienin A, influence the TNFR1 expression indirectly through ribotoxic stress response-induced ectodomain shedding [32,36,57,58]. Derivatives of the *Aglaia* flavagline rocaglamide influence the NF-κB activity by prohibiting the phosphorylation and subsequent degradation of IκBα in T cells, while vioprolide A again prevents the nuclear translocation of NF-κB through affecting nuclear import proteins [32,59]. Interestingly, HHT itself has previously been connected to the NF-κB signaling cascade: In dextran sulfate sodium-induced colitis, HHT has been shown to reduce the phosphorylation-dependent activation of NF-κB, while in K562 lymphoblast cells the protein level of NF-κB itself is decreased [30,60]. Surprisingly, in our study, we did not observe any connection between the anti-inflammatory effects of HHT and TNF-induced NF-κB signaling, since neither the activation of NF-κB nor its nuclear translocation were influenced.

Importantly, besides binding sites for NF-κB as transcription factor, the promotor region of *ICAM1* and *VCAM1* also contains binding sites for other transcription factors: The promotor region of *VCAM1* but not *ICAM1* also includes IRF-1 and GATA-6 binding domains [18,19]. IRF-1,

in turn, has been shown to be destabilized through excessive MAPK signaling [49]. Considering that HHT strongly enhanced the activation of the three MAPKs JNK, p38 and ERK1/2, we suggested that HHT might destabilize the *IRF1* mRNA. However, concurring with the *ICAM1* mRNA levels, IRF1 mRNA was strongly stabilized upon HHT treatment, which we could connect to the enhanced activation of p38. Still, the nuclear abundance of IRF-1 was drastically reduced in HHT-treated HUVECs, which we could trace back to an overall reduction of the IRF-1 total protein level. While we observed strong effects on the transcription factor IRF-1, HHT neither influenced the nuclear abundance nor the total protein level of GATA-6 after up to 4 h of treatment. Interestingly, in human coronary aortic smooth muscle cells, treatment with the translation elongation inhibitor cycloheximide (CHX) has been shown to reduce the GATA-6 protein level to approx. 50 % after 4 h already [61]. This suggests that, although HHT, like CHX, alters general *de novo* biosynthesis, the resulting effect size on different proteins differs widely.

In summary, the present study highlights the anti-inflammatory effects of the *Cephalotaxus* alkaloid and translation inhibitor HHT. These effects are evoked through effective inhibition of the leukocyte-endothelial cell interaction. Importantly, we demonstrated that the anti-inflammatory properties of HHT are not only evoked on the leukocyte side, but that the vascular endothelium is also of great importance.

Funding

This work was supported by the Hessisches Ministerium für Wissenschaft und Kunst, Landes offensive zur Entwicklung wissenschaftlich-ökonomischer Exzellenz (LOEWE) Center “Translational Biodiversity Genomics” (TBG), Germany. This work was also funded by the German Research Association (DFG) Graduate School 2336, project nr. 321115009, under the subproject (TP) TP09 and TP01.

CRediT authorship contribution statement

Robert Fürst: Writing – review & editing, Validation, Supervision, Resources, Project administration, Methodology, Funding acquisition, Data curation, Conceptualization. **Achim Schmidtko:** Writing – review & editing, Validation, Resources, Methodology. **Andreas Weigert:** Writing – review & editing, Validation, Resources, Methodology. **Tobias Schmid:** Writing – review & editing, Validation, Resources, Methodology. **Tobias Primke:** Writing – review & editing, Methodology, Investigation. **Anastasiia Kiprina:** Writing – review & editing, Methodology, Investigation. **Rebecca Raue:** Writing – review & editing, Methodology. **Silvia Kuntschar:** Writing – review & editing, Methodology. **Patrick Engel:** Writing – review & editing, Methodology, Investigation, Formal analysis. **Sarah Ciurus:** Writing – review & editing, Methodology, Investigation, Formal analysis, Conceptualization. **Luisa D. Burgers:** Writing – original draft, Visualization, Validation, Software, Methodology, Investigation, Formal analysis, Data curation, Conceptualization.

Declaration of Competing Interest

The authors declare that they have no known competing financial interests or personal relationships that could have appeared to influence the work reported in this paper.

Acknowledgement

We acknowledge the help of Mareike Lang and Isabelle Petith in performing western blot experiments.

Appendix A. Supporting information

Supplementary data associated with this article can be found in the online version at doi:10.1016/j.biopha.2024.116907.

References

[1] G. Caputa, A. Castoldi, E.J. Pearce, Metabolic adaptations of tissue-resident immune cells, Nat. Immunol. *20* (7) (2019) 793–801, https://doi.org/10.1038/s41590-019-0407-0.
[2] B.J. Hunt, K.M. Jurd, Endothelial cell activation. A central pathophysiological process, BMJ *316* (7141) (1998) 1328–1329, https://doi.org/10.1136/bmj.316.7141.1328.
[3] T.M. McIntyre, S.M. Prescott, A.S. Weyrich, G.A. Zimmerman, Cell-cell interactions: leukocyte-endothelial interactions, Curr. Opin. Hematol. *10* (2) (2003) 150–158, https://doi.org/10.1097/00062752-200303000-00009.
[4] M. Blonska, P.B. Shambharkar, M. Kobayashi, D. Zhang, H. Sakurai, B. Su, X. Lin, TAK1 is recruited to the tumor necrosis factor-alpha (TNF-alpha) receptor 1 complex in a receptor-interacting protein (RIP)-dependent manner and cooperates with MEKK3 leading to NF-kappaB activation, J. Biol. Chem. *280* (52) (2005) 43056–43063, https://doi.org/10.1074/jbc.M507807200.
[5] H. Wajant, P. Scheurich, TNFR1-induced activation of the classical NF-kappaB pathway. FEBS J. *278* (6) (2011) 862–876, https://doi.org/10.1111/j.1742-4658.2011.08015.x.
[6] C.B. Phelps, L.L. Sengchanthalangsy, T. Huxford, G. Ghosh, Mechanism of I kappa B alpha binding to NF-kappa B dimers, J. Biol. Chem. *275* (38) (2000) 29840–29846, https://doi.org/10.1074/jbc.M004899200.
[7] M. Karin, How NF-kappaB is activated: the role of the IkappaB kinase (IKK) complex, Oncogene *18* (49) (1999) 6867–6874, https://doi.org/10.1038/sj.onc.1203219.
[8] A.A. Beg, S.M. Ruben, R.I. Scheinman, S. Haskill, C.A. Rosen, A.S. Baldwin Jr., I kappa B interacts with the nuclear localization sequences of the subunits of NF-kappa B: a mechanism for cytoplasmic retention, Genes Dev. *6* (10) (1992) 1899–1913, https://doi.org/10.1101/gad.6.10.1899.
[9] R. Brignall, A.T. Moody, S. Mathew, S. Gaudet, Considering Abundance, Affinity, and Binding Site Availability in the NF-kappaB Target Selection Puzzle. Front Immunol. *10* (2019) 609, https://doi.org/10.3389/fimmu.2019.00609.
[10] T.M. Bui, H.L. Wiesolek, R. Sumagin, ICAM-1: A master regulator of cellular responses in inflammation, injury resolution, and tumorigenesis, J. Leukoc. Biol. *108* (3) (2020) 787–799, https://doi.org/10.1002/JLB.2MR0220-549R.
[11] D.H. Kong, Y.K. Kim, M.R. Kim, J.H. Jang, S. Lee, Emerging Roles of Vascular Cell Adhesion Molecule-1 (VCAM-1) in Immunological Disorders and Cancer, Int J. Mol. Sci. *19* (4) (2018), https://doi.org/10.3390/ijms19041057.
[12] S.R. Barthel, J.D. Gavino, L. Descheny, C.J. Dimitroff, Targeting selectins and selectin ligands in inflammation and cancer, Expert Opin. Ther. Targets *11* (11) (2007) 1473–1491, https://doi.org/10.1517/14728222.11.11.1473.
[13] R. Yan, M. van Meurs, E.R. Popa, R.M. Jongman, P.J. Zwiers, A.E. Niemarkt, T. Kuiper, J.A. Kamps, P. Heeringa, J.G. Zijlstra, G. Molema, J. Moser, Endothelial Interferon Regulatory Factor 1 Regulates Lipopolysaccharide-Induced VCAM-1 Expression Independent of NFkappaB. J. Innate Immun. *9* (6) (2017) 546–560, https://doi.org/10.1159/000477211.
[14] P. Fang, H.Y. Shi, X.M. Wu, Y.H. Zhang, Y.J. Zhong, W.J. Deng, Y.P. Zhang, M. Xie, Targeted inhibition of GATA-6 attenuates airway inflammation and remodeling by regulating caveolin-1 through TLR2/MyD88/NF-kappaB in murine model of asthma. Mol. Immunol. *75* (2016) 144–150, https://doi.org/10.1016/j.molimm.2016.05.017.
[15] X. Fan, X. Chen, Q. Feng, K. Peng, Q. Wu, A.G. Passerini, S.I. Simon, C. Sun, Downregulation of GATA6 in mTOR-inhibited human aortic endothelial cells: effects on TNF-alpha-induced VCAM-1 expression and monocytic cell adhesion, Am. J. Physiol. Heart Circ. Physiol. *316* (2) (2019) H408–H420, https://doi.org/10.1152/ajpheart.00411.2018.
[16] C. Anbarasan, M. Bavanilatha, K. Latchumanadhas, S. Ajit Mullasari, ICAM-1 molecular mechanism and genome wide SNP’s association studies, Indian Heart J. *67* (3) (2015) 282–287, https://doi.org/10.1016/j.ihj.2015.03.005.
[17] M. Ahmad, P. Theofanidis, R.M. Medford, Role of activating protein-1 in the regulation of the vascular cell adhesion molecule-1 gene expression by tumor necrosis factor-alpha, J. Biol. Chem. *273* (8) (1998) 4616–4621, https://doi.org/10.1074/jbc.273.8.4616.
[18] M.F. Iademarco, J.J. McQuillan, G.D. Rosen, D.C. Dean, Characterization of the promoter for vascular cell adhesion molecule-1 (VCAM-1), J. Biol. Chem. *267* (23) (1992) 16323–16329.
[19] A.S. Neish, A.J. Williams, H.J. Palmer, M.Z. Whitley, T. Collins, Functional analysis of the human vascular cell adhesion molecule 1 promoter, J. Exp. Med *176* (6) (1992) 1583–1593, https://doi.org/10.1084/jem.176.6.1583.
[20] D. Furman, J. Campisi, E. Verdin, P. Carrera-Bastos, S. Targ, C. Franceschi, L. Ferrucci, D.W. Gilroy, A. Fasano, G.W. Miller, A.H. Miller, A. Mantovani, C. M. Weyand, N. Barzilai, J.J. Goronzy, T.A. Rando, R.B. Effros, A. Lucia, N. Kleinstreuer, G.M. Slavich, Chronic inflammation in the etiology of disease across the life span, Nat. Med *25* (12) (2019) 1822–1832, https://doi.org/10.1038/s41591-019-0675-0.
[21] Y.Y. Li, T.M. Zollner, M.P. Schon, Targeting leukocyte recruitment in the treatment of psoriasis, Clin. Dermatol. *26* (5) (2008) 527–538, https://doi.org/10.1016/j.clindermatol.2007.11.002.
[22] L.P. McLean, T. Shea-Donohue, R.K. Cross, Vedolizumab for the treatment of ulcerative colitis and Crohn’s disease, Immunotherapy *4* (9) (2012) 883–898, https://doi.org/10.2217/imt.12.85.
[23] H.A. Blair, Crizanlizumab: First Approval, Drugs *80* (1) (2020) 79–84, https://doi.org/10.1007/s40265-019-01254-2.
[24] M. Fresno, A. Jimenez, D. Vazquez, Inhibition of translation in eukaryotic systems by harringtonine, Eur. J. Biochem *72* (2) (1977) 323–330, https://doi.org/10.1111/j.1432-1033.1977.tb11256.x.

[25] G. Gurel, G. Blaha, P.B. Moore, T.A. Steitz, U2504 determines the species specificity of the A-site cleft antibiotics: the structures of tiamulin, homoharringtonine, and bruceantin bound to the ribosome, J. Mol. Biol. *389* (1) (2009) 146–156, https://doi.org/10.1016/j.jmb.2009.04.005.
[26] L.D. Burgers, R. Furst, Natural products as drugs and tools for influencing core processes of eukaryotic mRNA translation, Pharm. Res *170* (2021) 105535, https://doi.org/10.1016/j.phrs.2021.105535.
[27] V. Gandhi, W. Plunkett, J.E. Cortes, Omacetaxine: a protein translation inhibitor for treatment of chronic myelogenous leukemia, Clin. Cancer Res *20* (7) (2014) 1735–1740, https://doi.org/10.1158/1078-0432.CCR-13-1283.
[28] M. Kim, H. Jo, Y. Kwon, Y. Kim, H.S. Jung, D. Jeoung, Homoharringtonine Inhibits Allergic Inflammations by Regulating NF-kappaB-miR-183-5p-BTG1 Axis. Front Pharm. *11* (2020) 1032, https://doi.org/10.3389/fphar.2020.01032.
[29] X. Jiang, Q. Wu, C. Zhang, M. Wang, Homoharringtonine Inhibits Alzheimer's Disease Progression by Reducing Neuroinflammation via STAT3 Signaling in APP/PS1 Mice, Neurodegener. Dis. *21* (3-4) (2021) 93–102, https://doi.org/10.1159/000519974.
[30] J. Liu, L. Shi, W. Huang, Z. Zheng, X. Huang, Y. Su, Homoharringtonine Attenuates Dextran Sulfate Sodium-Induced Colitis by Inhibiting NF-kappaB Signaling. Mediat. Inflamm. *2022* (2022) 3441357 https://doi.org/10.1155/2022/3441357.
[31] D.J. Medina-Leyte, M. Domínguez-Pérez, I. Mercado, M.T. Villarreal-Molina, L. Jacobo-Albavera, Use of Human Umbilical Vein Endothelial Cells (HUVEC) as a Model to Study Cardiovascular Disease: A Review, Appl. Sci. *10* (3) (2020) 938, https://doi.org/10.3390/app10030938.
[32] L.D. Burgers, B. Luong, Y. Li, M.P. Fabritius, S. Michalakis, C.A. Reichel, R. Muller, R. Furst, The natural product vioprolide A exerts anti-inflammatory actions through inhibition of its cellular target NOP14 and downregulation of importin-dependent NF-kB p65 nuclear translocation, Biomed. Pharm. *144* (2021) 112255, https://doi.org/10.1016/j.biopha.2021.112255.
[33] E.A. Jaffe, R.L. Nachman, C.G. Becker, C.R. Minick, Culture of human endothelial cells derived from umbilical veins. Identification by morphologic and immunologic criteria, J. Clin. Invest *52* (11) (1973) 2745–2756, https://doi.org/10.1172/JCI107470.
[34] A. Boyum, Isolation of lymphocytes, granulocytes and macrophages, Scand. J. Immunol. (*Suppl 5*) (1976) 9–15.
[35] N.S. Doherty, P. Poubelle, P. Borgeat, T.H. Beaver, G.L. Westrich, N.L. Schrader, Intraperitoneal injection of zymosan in mice induces pain, inflammation and the synthesis of peptidoleukotrienes and prostaglandin E2, Prostaglandins *30* (5) (1985) 769–789, https://doi.org/10.1016/0090-6980(85)90006-1.
[36] A. Stark, R. Schwenk, G. Wack, G. Zuchtriegel, M.G. Hatemler, J. Brautigam, A. Schmidtko, C.A. Reichel, I. Bischoff, R. Furst, Narciclasine exerts anti-inflammatory actions by blocking leukocyte-endothelial cell interactions and down-regulation of the endothelial TNF receptor 1, Faseb J. *33* (8) (2019) 8771–8781, https://doi.org/10.1096/fj.201802440R.
[37] A. Laux-Biehlmann, J. Boyken, H. Dahllof, N. Schmidt, T.M. Zollner, J. Nagel, Dynamic weight bearing as a non-reflexive method for the measurement of abdominal pain in mice, Eur. J. Pain. *20* (5) (2016) 742–752, https://doi.org/10.1002/ejp.800.
[38] E.J. Cobos, N. Ghasemlou, D. Araldi, D. Segal, K. Duong, C.J. Woolf, Inflammation-induced decrease in voluntary wheel running in mice: a nonreflexive test for evaluating inflammatory pain and analgesia, Pain *153* (4) (2012) 876–884, https://doi.org/10.1016/j.pain.2012.01.016.
[39] S. Rose, A. Misharin, H. Perlman, A novel Ly6C/Ly6G-based strategy to analyze the mouse splenic myeloid compartment, Cytom. A *81* (4) (2012) 343–350, https://doi.org/10.1002/cyto.a.22012.
[40] M. Cella, A. Engering, V. Pinet, J. Pieters, A. Lanzavecchia, Inflammatory stimuli induce accumulation of MHC class II complexes on dendritic cells, Nature *388* (6644) (1997) 782–787, 10.1038/42030.
[41] M. Baumgart, V. Moos, D. Schuhbauer, B. Muller, Differential expression of major histocompatibility complex class II genes on murine macrophages associated with T cell cytokine profile and protective/suppressive effects, Proc. Natl. Acad. Sci. USA *95* (12) (1998) 6936–6940, https://doi.org/10.1073/pnas.95.12.6936.
[42] I. Nicoletti, G. Migliorati, M.C. Pagliacci, F. Grignani, C. Riccardi, A rapid and simple method for measuring thymocyte apoptosis by propidium iodide staining and flow cytometry, J. Immunol. Methods *139* (2) (1991) 271–279, https://doi.org/10.1016/0022-1759(91)90198-o.
[43] A. Scholz, P. Rappl, N. Boffinger, A.C. Mota, B. Brune, T. Schmid, Translation of TNFAIP2 is tightly controlled by upstream open reading frames, Cell Mol. Life Sci. *77* (10) (2020) 2017–2027, https://doi.org/10.1007/s00018-019-03265-4.
[44] J.L. Cash, G.E. White, D.R. Greaves, Chapter 17. Zymosan-induced peritonitis as a simple experimental system for the study of inflammation, Methods Enzym. *461* (2009) 379–396, https://doi.org/10.1016/S0076-6879(09)05417-2.
[45] P. Shrikant, I.Y. Chung, M.E. Ballestas, E.N. Benveniste, Regulation of intercellular adhesion molecule-1 gene expression by tumor necrosis factor-alpha, interleukin-1 beta, and interferon-gamma in astrocytes. *J Neuroimmunol 51* (2) (1994) 209–220, https://doi.org/10.1016/0165-5728(94)90083-3.
[46] T. Wu, J.X. Shi, S. Geng, W. Zhou, Y. Shi, X. Su, The MK2/HuR signaling pathway regulates TNF-alpha-induced ICAM-1 expression by promoting the stabilization of ICAM-1 mRNA, BMC Pulm. Med. *16* (1) (2016) 84, https://doi.org/10.1186/s12890-016-0247-8.
[47] A. Lugowski, B. Nicholson, O.S. Rissland, Determining mRNA half-lives on a transcriptome-wide scale, Methods *137* (2018) 90–98, https://doi.org/10.1016/j.ymeth.2017.12.006.
[48] H.C. Ledebur, T.P. Parks, Transcriptional regulation of the intercellular adhesion molecule-1 gene by inflammatory cytokines in human endothelial cells. Essential roles of a variant NF-kappa B site and p65 homodimers, J. Biol. Chem. *270* (2) (1995) 933–943, https://doi.org/10.1074/jbc.270.2.933.
[49] S. Shah, E.M. King, M.M. Mostafa, M.O. Altonsy, R. Newton, DUSP1 Maintains IRF1 and Leads to Increased Expression of IRF1-dependent Genes: a mechanism promoting glucocorticoid insensitivity, J. Biol. Chem. *291* (41) (2016) 21802–21816, https://doi.org/10.1074/jbc.M116.728964.
[50] D.P. Franco, B.I. de Biazi, T.A. Zanetti, L.A. Marques, L. de Lima, S.R. Lepri, M. S. Mantovani, Apoptotic and cell cycle response to homoharringtonine and harringtonine in wild and mutant p53 hepatocarcinoma cells, Hum. Exp. Toxicol. *39* (10) (2020) 1405–1416, https://doi.org/10.1177/0960327120926257.
[51] T.L. Jiang, R.H. Liu, S.E. Salmon, Comparative in vitro antitumor activity of homoharringtonine and harringtonine against clonogenic human tumor cells, Invest N. Drugs *1* (1) (1983) 21–25, https://doi.org/10.1007/BF00180188.
[52] C.Y. Chen, A.B. Shyu, AU-rich elements: characterization and importance in mRNA degradation, Trends Biochem Sci. *20* (11) (1995) 465–470, https://doi.org/10.1016/s0968-0004(00)89102-1.
[53] A. Sidali, V. Teotia, N.S. Solaiman, N. Bashir, R. Kanagaraj, J.J. Murphy, K. Surendranath, AU-rich element RNA binding proteins: at the crossroads of post-transcriptional regulation and genome integrity, Int. J. Mol. Sci. *23* (1) (2021), https://doi.org/10.3390/ijms23010096.
[54] A.C. Vind, A.V. Genzor, S. Bekker-Jensen, Ribosomal stress-surveillance: three pathways is a magic number, Nucleic Acids Res *48* (19) (2020) 10648–10661, https://doi.org/10.1093/nar/gkaa757.
[55] S. De, O. Muhlemann, A comprehensive coverage insurance for cells: revealing links between ribosome collisions, stress responses and mRNA surveillance, RNA Biol. *19* (1) (2022) 609–621, https://doi.org/10.1080/15476286.2022.2065116.
[56] N. Garreau de Loubresse, I. Prokhorova, W. Holtkamp, M.V. Rodnina, G. Yusupova, M. Yusupov, Structural basis for the inhibition of the eukaryotic ribosome, Nature *513* (7519) (2014) 517–522, https://doi.org/10.1038/nature13737.
[57] Y. Yamada, S. Taketani, H. Osada, T. Kataoka, Cytotrienin A, a translation inhibitor that induces ectodomain shedding of TNF receptor 1 via activation of ERK and p38 MAP kinase, Eur. J. Pharm. *667* (1-3) (2011) 113–119, https://doi.org/10.1016/j.ejphar.2011.05.072.
[58] Y. Yamada, E. Tashiro, S. Taketani, M. Imoto, T. Kataoka, Mycotrienin II, a translation inhibitor that prevents ICAM-1 expression induced by pro-inflammatory cytokines, J. Antibiot. *64* (5) (2011) 361–366, https://doi.org/10.1038/ja.2011.23.
[59] B. Baumann, F. Bohnenstengel, D. Siegmund, H. Wajant, C. Weber, I. Herr, K. M. Debatin, P. Proksch, T. Wirth, Rocaglamide derivatives are potent inhibitors of NF-kappa B activation in T-cells, J. Biol. Chem. *277* (47) (2002) 44791–44800, https://doi.org/10.1074/jbc.M208003200.
[60] L.L. Ye, W.K. Cao, Y.Y. Shi, Z.K. Deng, S.D. Tao, P. Ji, X.H. Fu, M.Z. Zong, Y.F. Li, Effect of homoharringtonine on expression of NF-kappaB and BCL-2 proteins in K562 cells]. Zhongguo Shi Yan Xue Ye Xue Za Zhi *21* (1) (2013) 78–81, https://doi.org/10.7534/j.issn.1009-2137.2013.01.017.
[61] Y. Xie, Y. Jin, B.L. Merenick, M. Ding, K.M. Fetalvero, R.J. Wagner, A. Mai, S. Gleim, D.F. Tucker, M.J. Birnbaum, B.A. Ballif, A.K. Luciano, W.C. Sessa, E. M. Rzucidlo, R.J. Powell, L. Hou, H. Zhao, J. Hwa, J. Yu, K.A. Martin, Phosphorylation of GATA-6 is required for vascular smooth muscle cell differentiation after mTORC1 inhibition, Sci. Signal *8* (376) (2015) ra44, https://doi.org/10.1126/scisignal.2005482.